RESEARCH ARTICLE

Neonatal therapy with PF543, a sphingosine kinase 1 inhibitor, ameliorates hyperoxia-induced airway remodeling in a murine model of bronchopulmonary dysplasia

Alison W. Ha,[1]* Tara Sudhadevi,[2]* David L. Ebenezer,[3] Panfeng Fu,[3] Evgeny V. Berdyshev,[4] Steven J. Ackerman,[1] Viswanathan Natarajan,[3,5] and Anantha Harijith[2]

[1]*Department of Biochemistry, University of Illinois, Chicago, Illinois;* [2]*Department of Pediatrics, Case Western Reserve University, Cleveland, Ohio;* [3]*Department of Pharmacology, University of Illinois, Chicago, Illinois;* [4]*Department of Medicine, National Jewish Health, Denver, Colorado; and* [5]*Department of Medicine, University of Illinois, Chicago, Illinois*

Ha AW, Sudhadevi T, Ebenezer DL, Fu P, Berdyshev EV, Ackerman SJ, Natarajan V, Harijith A. Neonatal therapy with PF543, a sphingosine kinase 1 inhibitor, ameliorates hyperoxia-induced airway remodeling in a murine model of bronchopulmonary dysplasia. *Am J Physiol Lung Cell Mol Physiol* 319: L497–L512, 2020. First published July 22, 2020; doi:10.1152/ajplung.00169. 2020.—Hyperoxia (HO)-induced lung injury contributes to bronchopulmonary dysplasia (BPD) in preterm newborns. Intractable wheezing seen in BPD survivors is associated with airway remodeling (AWRM). Sphingosine kinase 1 (SPHK1)/sphingosine-1-phosphate (S1P) signaling promotes HO-mediated neonatal BPD; however, its role in the sequela of AWRM is not known. We noted an increased concentration of S1P in tracheal aspirates of neonatal infants with severe BPD, and earlier, demonstrated that $Sphk1^{-/-}$ mice showed protection against HO-induced BPD. The role of SPHK1/S1P in promoting AWRM following exposure of neonates to HO was investigated in a murine model. Therapy using PF543, the specific SPHK1 inhibitor, during neonatal HO reduced alveolar simplification followed by reduced AWRM in adult mice. This was associated with reduced airway hyperreactivity to intravenous methacholine. Neonatal HO exposure was associated with increased expression of SPHK1 in lung tissue of adult mice, which was reduced with PF543 therapy in the neonatal stage. This was accompanied by amelioration of HO-induced reduction of E-cadherin in airway epithelium. This may be suggestive of arrested partial epithelial mesenchymal transition (EMT) induced by HO. In vitro studies using human primary airway epithelial cells (HAEpCs) showed that SPHK1 inhibition or deletion restored HO-induced reduction in E-cadherin and reduced formation of mitochondrial reactive oxygen species (mtROS). Blocking mtROS with MitoTempo attenuated HO-induced partial EMT of HAEpCs. These results collectively support a therapeutic role for PF543 in preventing HO-induced BPD in neonates and the long-term sequela of AWRM, thus conferring a long-term protection resulting in improved lung development and function.

airway remodeling; bronchopulmonary dysplasia; mitochondrial ROS; PF543; sphingosine kinase 1

INTRODUCTION

Bronchopulmonary dysplasia (BPD) continues to be a debilitating chronic lung condition affecting the preterm newborn, adding significantly to the health care burden (54). Preterm birth affects nearly 500,000 babies every year in North America, and its incidence has risen by 36% over the past 25 years (64). Because of advances in medical care, the survival rate of extreme low birth weight infants (defined by birth weight <1,000 g) has dramatically increased (53). However, this increased survival is accompanied by an increased prevalence of morbidity, dominated by BPD and its accompanying sequelae (31, 54). About 25–40% of extreme low birth weight preterm newborns develop BPD. BPD is a clinical diagnosis based on the need for supplemental oxygen at 36 wk of postmenstrual age (29). Although exposure of preterm neonates to oxygen supplementation or hyperoxia (HO) reduces mortality, an unintended outcome is that it contributes to poor lung development, leading to BPD characterized by poorly formed alveoli and airway remodeling (AWRM). It was long believed by physicians that BPD would get corrected with age due to compensatory lung growth (45). But recent scientific evidence has negated this notion. Even mild BPD is known to cause impairment of lung function in childhood (19). Recent reports indicate that wheezing in BPD is poorly responsive to bronchodilators due to adverse AWRM leading to narrowing of the airways (16, 60). The insult received at birth has its impact for life, with survivors of BPD suffering from wheezing disorders, increased incidence of pneumonia, declining lung function, pulmonary hypertension, learning disabilities, and neurological disorders (13, 54). Thus, the combination of remodeled narrow airways and poorly formed alveoli causing deprivation of oxygen to the whole body has a crippling effect on BPD survivors. Despite recent progress in understanding the pathophysiology of BPD, there have been no real therapeutic solutions.

In our previous studies, we showed that under hyperoxic conditions, $Sphk1^{-/-}$ mice were protected against alveolar simplification (BPD morphology) in neonates, and lung injury in adults (21, 22). We demonstrated that use of PF543, a specific inhibitor of sphingosine kinase 1 (SPHK1), prevented generation of intracellular reactive oxygen species (ROS) which conferred protection against HO (21). While the long-

---

term consequences of HO exposure and BPD is known, the impact of a therapy during neonatal hyperoxia in improving adult lung function has not been investigated. This study is primarily aimed at addressing this lacuna. Airway hyperreactivity (AHR) is caused by AWRM in patients with BPD. Significant aspects of AWRM include morphological changes in airway smooth muscle, such as hypertrophy /hyperplasia, and peribronchial fibrosis.

According to Barker's hypothesis, the roots of adult health disorders lie in fetal/neonatal illness (3, 11). In line with this hypothesis, this study examined the impact of PF543 therapy during neonatal hyperoxic insult in reducing AWRM in adults. We focused on characterizing the airway structure and AHR using murine model of BPD. The role of epithelial mesenchymal transition (EMT) in the pathogenesis of AWRM was also investigated using lung tissue and airway epithelial cells. We have shown for the first time that treatment with PF543 during exposure to HO as a neonate is associated with reduced AWRM and AHR in adults. The studies presented here clearly demonstrate the impact of PF543 therapy during neonatal hyperoxic stress lasting into adulthood.

MATERIALS AND METHODS

Human lung tracheal aspirate collection. Tracheal aspirates (TAs) were collected from premature infants being mechanically ventilated with an in-dwelling endotracheal tube. Collection and processing of human TAs were approved by the Institutional Review Board of the University of Illinois at Chicago (protocol no. 2010-1111, "Consortium for Neonatal Intensive Care Unit"), and consent from both parents was obtained before collection. TAs were collected cross sectionally from controls born at term and those meeting criteria of mild, moderate, or severe BPD when endotracheal tube lavage was performed as part of routine care. Samples from a total of 18 patients were analyzed. Term healthy infants (controls) were intubated for elective procedures such as repair of myelomeningocele, bilateral hydronephrosis with posterior urethral valve, inguinal hernia, gastroschisis, or anorectal malformation. They had no pulmonary conditions. Aspirate specimens were centrifuged and supernatants were stored at $-80°C$. BPD and its severity were defined as per NIH consensus criteria (29). Select clinical details are shown in Table 1.

S1P was measured by tandem mass spectrometry. S1P concentration was corrected and normalized to the total lipid phosphorous of the TA total lipid extract. Bulk of S1P in plasma is primarily bound to the HDL fraction of cholesterol. S1P is a lysophospholipid, and its concentration of S1P is independent of the total protein concentration. Samples contaminated with mucus, blood, and residual debris or with very low number of cells were discarded. All infants in the study were followed until 36 wk of postmenstrual age or discharge, whichever was later. Investigators involved in biomarker measurements were blinded to the patient characteristics and outcomes.

Analysis of sphingoid base-1-phosphates. We used electrospray ionization tandem mass spectrometry (ESI-LC/MS/MS) to analyze these phospholipids (22). API4000 Q-trap hybrid triple quadrupole linear ion-trap mass spectrometer (Applied Biosystems, Foster City, CA) equipped with a turbo ion spray ionization source interfaced with an automated Agilent 1100 series liquid chromatograph and auto sampler (Agilent Technologies, Wilmington, DE) was used. S1P and DH-S1P were analyzed as *bis*-acetylated derivatives with C17-S1P used as the internal standard employing reverse-phase HPLC separation, negative ion ESI, and MRM analysis.

Mouse experiments and animal care. All experiments using animals were approved by the Institutional Animal Care and Use Committee at the University of Illinois at Chicago (protocol no. 15-240). C57BL/6J (WT) mice were used to investigate the role of PF543 in neonatal lung injury and AWRM. As previously reported, neonatal pups with their lactating dams were used (22). Dams were rotated between HO and room air (RA) every 24 h. After birth, the pups and dams were randomized to RA group or HO group (95%). PF543 (5 mg/kg per dose) or vehicle was administered to the pups intraperitoneally on alternate days from postnatal (PN) 3 to PN 10 while being exposed to HO or RA. A total of four doses of PF543 or vehicle were given. Dosing experiments were performed with PF543 treatments ranging from 2 mg/kg per dose to 20 mg/kg (data not shown). The lowest effective dose that prevented HO-induced lung injury was 5 mg/kg per dose given intraperitoneally on alternate days, while no toxicity to the animals was noted at higher doses. Following exposure to HO or RA, the pups were either euthanized on PN 10 or allowed to grow in RA until 8 wk of age. The adult mice were used for lung function studies or histology and bronchoalveolar lavage (BAL). Both male and female mice were used in all experiments. Six to ten mice were used in each of the experiments and representative data are shown.

Table 1. *Selected information on the patients from whom tracheal aspirates were collected*

Severity of BPD	GA at Birth, wk	Birth Weight, g	Race	Sex	Cumulative Days on Oxygen	Corrected GA at S1P Measurement	C18-S1P Level, pmol/L	C18-DH S1P level, pmol/L	Wheezing Requiring β_2 Agonist Therapy
Severe	24 ± 2	550	AA	F	126	39 ± 2	11.46	1.01	Y
Severe	24 ± 5	720	AA	F	112	38 ± 1	12.1	3.0	Y
Severe	28 ± 2	960	AA	M	103	39 ± 5	6.04	0.38	Y
Severe	27 ± 6	1,000	AA	F	108	37	10.45	1.71	Y
Severe	28	1,090	H	M	103	37 ± 3	6.4	0.46	Y
Mild	26 ± 2	760	AA	M	42	27	2.0	1.17	N
Mild	25 ± 5	830	AA	F	45	27 ± 1	1.62	1.05	N
Mild	26 ± 5	950	H	M	48	30 ± 4	3.05	0.22	N
Mild	26 ± 6	1,000	H	M	36	27	3.64	0.59	N
Preterm no BPD	29 ± 5	1,250	AA	M	14	30 ± 3	1.42	0.79	N
Preterm no BPD	28	950	AA	F	22	28 ± 4	1.3	0.56	N
Preterm no BPD	30 ± 2	1,100	H	F	6	30 ± 4	1.3	0.4	N
Preterm no BPD	28 ± 1	910	H	M	16	29	1.7	2	N
Term Normal	39 ± 3	2,370	AA	M	0	39 ± 3	1.1	0	N
Term Normal	37	2,570	H	M	0	37	0.1	0	N
Term Normal	38	3,100	H	F	1	38	0.5	0	N
Term Normal	37	3,130	C	M	0	37	0.4	0	N
Term Normal	38 ± 2	3,410	H	M	2	38 ± 3	0.9	0	N

Values are means $\pm$ SE. AA, African-American; BPD, bronchopulmonary dysplasia; C, Caucasian; DH-S1P, dihydro-sphingosine 1-phosphate; GA, gestational age; H, Hispanic; S1P, sphingosine-1-phosphate; Y, yes; N, no.

Bronchoalveolar lavage collection and analysis. Mice were euthanized and BAL collection with PBS was undertaken, as described previously (21, 22). Protein concentrations in BAL fluid were measured using Bio-Rad Protein Assay (Bio-Rad, Hercules, CA) (21). Hydrogen peroxide (H_2O_2) level was measured in the BAL immediately after collection using an Amplex Red hydrogen peroxide/peroxidase assay kit (Invitrogen, Eugene, OR) (21).

Lung preparation for histology. Eight-week-old mice were intubated via the trachea and lungs collected for histology. The left lung lobe was inflated with 10% formaldehyde (pH 7.4, at a pressure of 20 cm H_2O), followed by fixation for a minimum of 24 h, and processed for paraffin embedding and sectioning. Lung tissue sections (5 μm thick) were used for subsequent analyses after hematoxylin and eosin (HE) staining or airway analyses after Masson's trichrome and Alcian blue-periodic acid-Schiff (PAS) staining or immunohistochemistry. Masson's trichrome detects fibrosis by staining collagen blue, and PAS detects goblet cell metaplasia by staining mucus red. Immunohistochemistry was done to assess the expression of SPHK1 (Abcam, San Francisco, CA), myosin using smooth muscle myosin heavy chain 11 antibody (Abcam), E-cadherin (Cell Signaling, Danvers, MA), or vimentin (Cell Signaling) and counterstained with hematoxylin. The stained sections were analyzed using Aperio/Halo system positive pixel count algorithm as intensity of strong positive staining was divided by area (mm^2).

Morphometric analysis of AWRM. The objective assessment of alveolarization was determined by the mean linear intercept (MLI) method, as described earlier (21, 22). Slides were scanned on a Leica Aperio AT2 whole slide scanner. To assess AWRM, regions of interest around the bronchus were drawn in Leica Aperio Imagescope v. 12.3.1.5011 (Leica Biosystems, Buffalo Grove, IL). These regions were then imported into Indica Labs Halo v. 2.0.1145.21. For peribronchial analyses, Masson's trichrome-stained airways were analyzed by tracing the epithelial and subepithelial layers over a 50-μm region around the bronchus followed by expression of the values as square micrometers per micrometer basement membrane length. Scoring was performed by examining at least 20 airways per section. Whole lung images were analyzed for quantification using Halo software (Indica Labs, Albuquerque, NM). The percentage of the region of interest that contained fibrosis was used as the outcome measure. For airway analyses, all images of bronchi were selected (measuring 150 to 350 μm luminal diameter) in a single section from each across the entire tissue sample, so that maximum airways were included for analyses. Similar method was used for SPHK1, E-cadherin, and vimentin. We analyzed stained sections using Aperio-positive pixel count algorithm as intensity of strong positive staining divided by area (mm^2). Myosin staining was assessed in the peribronchial region similar to the method used for Masson's trichrome staining assessment. The mean pixel density of room air exposed animals was taken as one and the intensity of expression of the given protein for the remaining groups were expressed as a fold change normalized to that of room air. Analyses of the size of airway caliber were performed. To correct for size of the airways, the outer diameter and the luminal diameter were measured. The luminal diameter was expressed as a percentage of the outer diameter.

Lung function studies and methacholine challenge. Methacholine challenge experiments were performed at 8 wk of age, as described earlier using flexiVent ventilator system (flexiVent; SCIREQ, Tempe, AZ) (8). Each mouse was challenged with increasing doses of methacholine (0, 2.5, 5, 10, 20, and 40 μg) intravenously through the jugular vein. At baseline and after each challenge, Respiratory system resistance (R_{rs}), which is an indicator of total lung resistance, Newtonian resistance (R_n), representing the resistance of the central or conducting airways, lung tissue impedance parameters, such as tissue resistance (G) and tissue elastance (H) were recorded during tidal breathing as programmed in the flexiVent system. Mean values of R_{rs}, R_n, G, and H were taken and expressed as shown in the graphs.

Materials. Primary human small airway epithelial cells (SAECs), SAGM media, and Bullet kit were obtained from Lonza (San Diego, CA), (CC - 2547, lot no. 0000494601, a 19-yr-old Caucasian female, nonsmoker and healthy, lot no. 0000669507, a 47-yr-old Caucasian male, healthy nonsmoker, lot no. TL 18037, a 45-yr-old African-American male). Authentication was done using cell type-specific staining by cytokeratin 19. Phosphate-buffered saline (PBS) was obtained from Biofluids. (Rockville, MD). Fetal bovine serum (FBS), trypsin, Triton X-100, and Tween 20, were obtained from Sigma-Aldrich Inc. (St. Louis, MO).

Infection of human primary airway epithelial cells with adenoviral vectors. Infection of human primary airway epithelial cells (~60% confluence) was accomplished with purified adenoviral empty vectors, and FLAG-tagged adenoviral vectors containing cDNA for *Sphk1* wild type (WT) or catalytically inactive *Sphk1* plasmid mutant were carried out in six-well plates, as described previously (63). After infection with different MOI in 1 ml of complete medium for 24 h, the virus containing medium was replaced with basal medium, and the experiments were carried out.

Exposure of cells to hyperoxia. The primary human small airway epithelial cells (SAECs) and the small airway growth medium (SAGM) complete media (10% FBS, 100 units/mL penicillin, and streptomycin) were obtained from Lonza, San Diego, CA. The cells at P4-P7 were used for the experiments. The cells were cultured in 35- or 60-mm dishes or chamber slides for various studies. For induction of HO, the cells in media (~90% confluence) were placed in a humidity-controlled airtight modulator incubator chamber (Billups-Rothenberg, Del Mar, CA), flushed continuously with 95% O_2-5% CO_2 for 30 min until the oxygen level inside the chamber reached ~95%. SAECs were then placed in the cell culture incubator at 37°C for 24 h of HO exposure. The concentration of O_2 inside the chamber was monitored with a digital oxygen monitor. The buffering capacity of the cell culture medium did not change significantly during the period of HO exposure and was maintained at a pH ~7.4.

Treatment of cells with SPHK1 inhibitor, PF543. SAECs were pretreated for 1 h with vehicle or PF543 (1 μM) (Cayman Chemical, Ann Arbor, MI) in media containing 1% FBS before stimulation with HO (95% for 24 h). Cells with the same treatment under RA served as controls. To study the effect of PF543 on mitochondrial ROS (mtROS) production, the cells were treated with 5 μM MitoSOX Red dye (ex/em λ = 510 nm/580 nm) for 10 min in dark, and live cell imaging was performed using confocal microscope, as already described (51). To examine the effect of PF543 on expression of EMT markers, such as E-cadherin and vimentin, the treated cells were processed for immunofluorescence.

Treatment of cells with mitochondrial superoxide scavenger MitoTEMPO. SAECs were pretreated with MitoTEMPO (Alexis Corporation, San Diego, CA) (10 μM) or solvent (vehicle) control for 2 h and subjected to RA or HO for 24 h and then stained for MitoSOX or EMT markers such as E-cadherin and vimentin.

Immunofluorescence staining and image analysis. SAECs grown on chamber slides (Millipore Temecula, CA) were exposed to RA or HO (95% O_2) for 24 h. Cells were fixed and subjected to immunostaining for E-cadherin, as well as vimentin, and image analysis was performed as described (21). IgG and secondary antibody-only controls were used. Incubation with E-cadherin (1:500 dilution) or vimentin antibody (1:500 dilution) was performed in blocking solution at room temperature for 1 h followed by staining with Alexa Fluor 488-conjugated secondary antibody (Molecular Probe, Eugene, OR). After immunostaining, slides were examined with Zeiss Laser Scanning Confocal Microscope (LSM) 710 META (Zeiss scanning systems, Maple Grove, MN) using ×60 oil-immersion objective lens. E-cadherin distribution at cell periphery or vimentin cytoskeleton expression within the cell were quantified using ImageJ algorithm, and a minimum of 20 typical cells (five different fields) from each experimental condition was analyzed for antibody distribution.

Statistical analysis. Histological and morphometric data were analyzed by GraphPad Prism (GraphPad Software, San Diego, CA). Student's *t* test or ANOVA was used to compare means of two or more different treatment groups respectively to assess the significance of the results. The level of significance is indicated as $P < 0.0001$, $P < 0.001$, $P < 0.01$, and $P \leq 0.05$. Results are expressed as means ± SE.

RESULTS

S1P concentration in human tracheal aspirates. Elevated S1P has been reported in patients with asthma (2) and BPD (23) and plays an important role in AWRM (17). In this context, we measured S1P in a cross-sectional study collecting TAs from patients with various stages of BPD and controls. Patients with severe BPD had elevated S1P levels in TAs (9.28 ± 1.28 pmol/mL) compared with those with mild BPD (2.58 ± 0.47 pmol/mL), preterm with no BPD (1.43 ± 0.95 pmol/mL), or normal term controls (mean 0.6 pmol/mL ± 0.18) (Fig. 1). While DH-S1P levels could be determined in preterm infants with and without BPD, the levels were, however, not detectable in normal term controls. Although the levels of DH-S1P were relatively higher in severe BPD compared with mild BPD, the differences were not significant. All the patients with severe BPD had symptomatic wheezing that was treated with albuterol. The patient information is summarized in Table 1.

The above data reveal elevated S1P levels in BPD. Our patient population was mostly African-American or of Hispanic origin, a reflection of the communities served by the University of Illinois Medical Center, Chicago. It should be noted that patients with severe BPD were intubated for a relatively long period with cumulative oxygen therapy of over 100 days. The patients had significant wheezing that partially responded to albuterol inhalation therapy. To further study the role of S1P in BPD/AWRM and subsequent role of SPHK1 inhibitor therapy, we used a murine model exposed to hyperoxia (42).
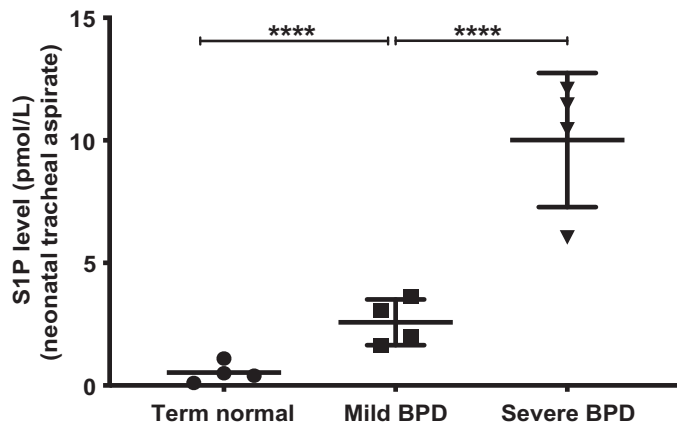

Fig. 1. Elevated sphingosine-1-phosphate (S1P) in tracheal aspirates (TA) of neonates was associated with severe bronchopulmonary dysplasia (BPD). TA collected from patients at various stages of BPD as well as term controls were analyzed for S1P (*n* = 18). Patients with established severe BPD (*n* = 5) and mild BPD (*n* = 4) had significantly elevated S1P levels compared with term controls (*n* = 5). Patients with severe BPD had significantly increased concentration of S1P in the TA compared with the rest of samples. The samples were collected as a cross-sectional study.

Immediate impact of PF543 treatment in neonatal mice exposed to hyperoxia. Our previous work clearly demonstrated that $Sphk1^{-/-}$ neonatal pups offered significant resistance to HO-induced lung injury (22). As an initial step, we administered SPHK1 inhibitor PF543 (5 mg/kg ip per dose) to mice exposed to either RA (21%) or HO (95%) on alternate days starting from PN 3. Administration of vehicle alone served as control. Following 7 days of HO, impaired alveolar formation was noted in the neonatal mice compared with RA controls. This was characterized by decreased number of alveoli that were larger and simplified. PF543 therapy ameliorated impaired alveolarization, as evidenced by reduced mean linear intercept (MLI) compared with untreated controls exposed to HO (Fig. 2, *A* and *B*). Quantitative analysis confirmed a reduction in alveolar size by almost 40% in the PF543-treated group exposed to HO (MLI of 42.0 ± 1.30 μm) compared with untreated HO-exposed mice (MLI of 64 ± 1.1 μm) and RA controls treated with vehicle (MLI of 34.2 ± 0.58 μm) or PF543 (MLI of 33.2 ± 1.03 μm). This was accompanied by reduced inflammation, as evidenced by reduced protein concentration in BAL collected from the lungs of neonatal mice exposed to HO and administered PF543 (0.55 ± 0.02 mg/mL) compared with similar mice treated with vehicle (0.87 ± 0.38 mg/mL) (Fig. 2*C*). The protein levels in BAL of RA vehicle group was not statistically different compared with similar group treated with PF543 (0.22 ± 0.01 vs. 0.23 ± 0.01 mg/mL). HO caused significant elevation of total cell count in BAL (344 ± 12.58 × 10^3/mL) compared with RA controls (45.8 ± 1.66 × 10^3/mL), and treatment with PF543 in the HO group reduced the total cell count (219.4 ± 7.06 × 10^3/mL) (Fig. 2*D*). BAL from neonatal mice on PN 10 showed increased H_2O_2 levels immediately at the end of HO (5.89 ± 0.9 μM) compared with RA controls (0.77 ± 0.02 μM) and RA pups treated with PF543 (0.81 ± 0.02 μM). PF543 therapy conferred protection against HO-induced alveolar simplification and was associated with reduced H_2O_2 production (2.94 ± 0.2 μM). This shows that inhibition of SPHK1 using PF543 during HO reduced H_2O_2 production (Fig. 2*E*). No difference was noted between males and females. As expected, therapy with PF543 reduced the plasma S1P levels (mean 534 ± 94 pmol/mL) significantly at the completion of the therapy on PN10 compared with controls treated with vehicle (mean 1056 ± 33 pmol/mL) (Fig. 2, *F* and *G*). PF543 also reduced the plasma DH-S1P levels (mean 284 ± 28 pmol/mL) significantly at the completion of the therapy on PN 10 compared with controls treated with vehicle (mean 109 ± 26 pmol/mL) (Fig. 2*G*).

Neonatal hyperoxia followed by lung development into adulthood. Impact of neonatal HO on lung architecture persisted into adulthood. Alveoli continued to show enlarged diameter at PN 56 in the neonatal HO-treated group (MLI of 61.6 ± 1.23 μm) compared with RA controls (MLI of 32.6 ± 1.03 μm) (Fig. 3, *A* and *B*). However, the protection seen in the neonates following PF543 therapy also persisted in adults, as evidenced by reduced BAL protein concentration in the HO-exposed and PF543-treated group (0.32 ± 0.01 mg/mL), as compared with HO control (0.43 ± 0.05 mg/mL) (Fig. 3*C*). The total WBC cell count in BAL showed a similar pattern. Neonatal HO exposed with a cell count of 0.43 ± 0.05 × 10^3/mL, whereas HO treated with PF543 during neonatal HO had a cell count of 0.32 × 10^3/mL ± SE 0.01) (Fig. 3*D*). In
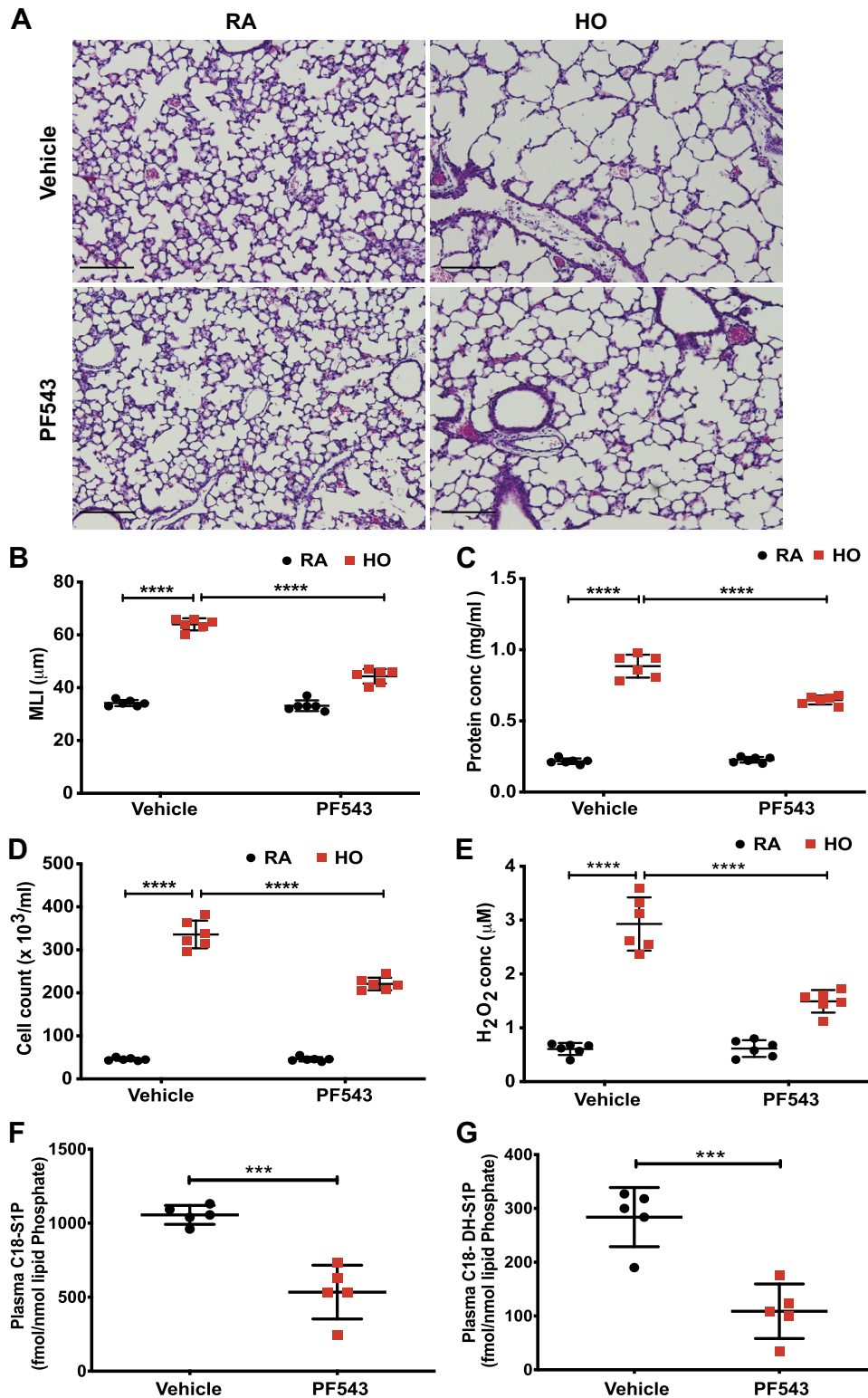
Fig. 2. Inhibition of sphingosine kinase 1 (SPHK1) with PF543 protects alveolarization of murine neonatal lungs under hyperoxia (HO) accompanied by reduced HO-induced inflammatory changes and H_2O_2 in bronchoalveolar lavage (BAL). *A*: representative H&E photomicrographs of lung sections obtained from wild-type (WT) mice treated with vehicle or PF543, exposed to RA or HO. PF543-treated newborn mice showed significantly improved alveolarization under HO compared with vehicle treated. *B*: objective assessment of alveolarization of neonatal lungs was determined by the mean linear intercept (MLI) method. Following exposure to HO, lung MLI in PF543-treated newborn mice was significantly lower compared with vehicle control exposed to HO, with significant decrease in BAL total protein levels (*C*), decreased total cell count (*D*), and decreased BAL hydrogen peroxide concentration (*E*). Plasma from vehicle and PF543-treated newborn mice were analyzed for S1P levels by LC/MS/MS. Both sphingosine 1-phosphate (S1P) and dihydro-sphingosine 1-phosphate (DH S1P) concentration were significantly lower in PF543-treated group compared with the vehicle treated (*F* and *G*). Original view, ×10, scale bar 100 μm. Statistical analyses were done with ANOVA test. ****$P < 0.0001$, ***$P < 0.001$; $n = 6–8$/group. Equal numbers of male and female mice were used.

addition, H_2O_2 was measured in the BAL of adults who were exposed to RA or HO as neonates (PN 3–10 at 95%) and treated with vehicle or PF543, as described earlier. There was no significant difference in the level of H_2O_2 in BAL among the adults exposed to HO as newborns (Fig. 3*E*). No difference was noted between males and females.

Analysis of airway remodeling and BAL. AWRM airway remodeling was assessed using *1*) subepithelial/peribronchial fibrosis (Masson's Trichrome) *2*) goblet cell metaplasia (Periodic acid-Schiff), and *3*) thickness of muscle layer (smooth muscle myosin heavy chain 11 antibody). There was no evidence of peribronchial fibrosis in the lungs of neonatal pups
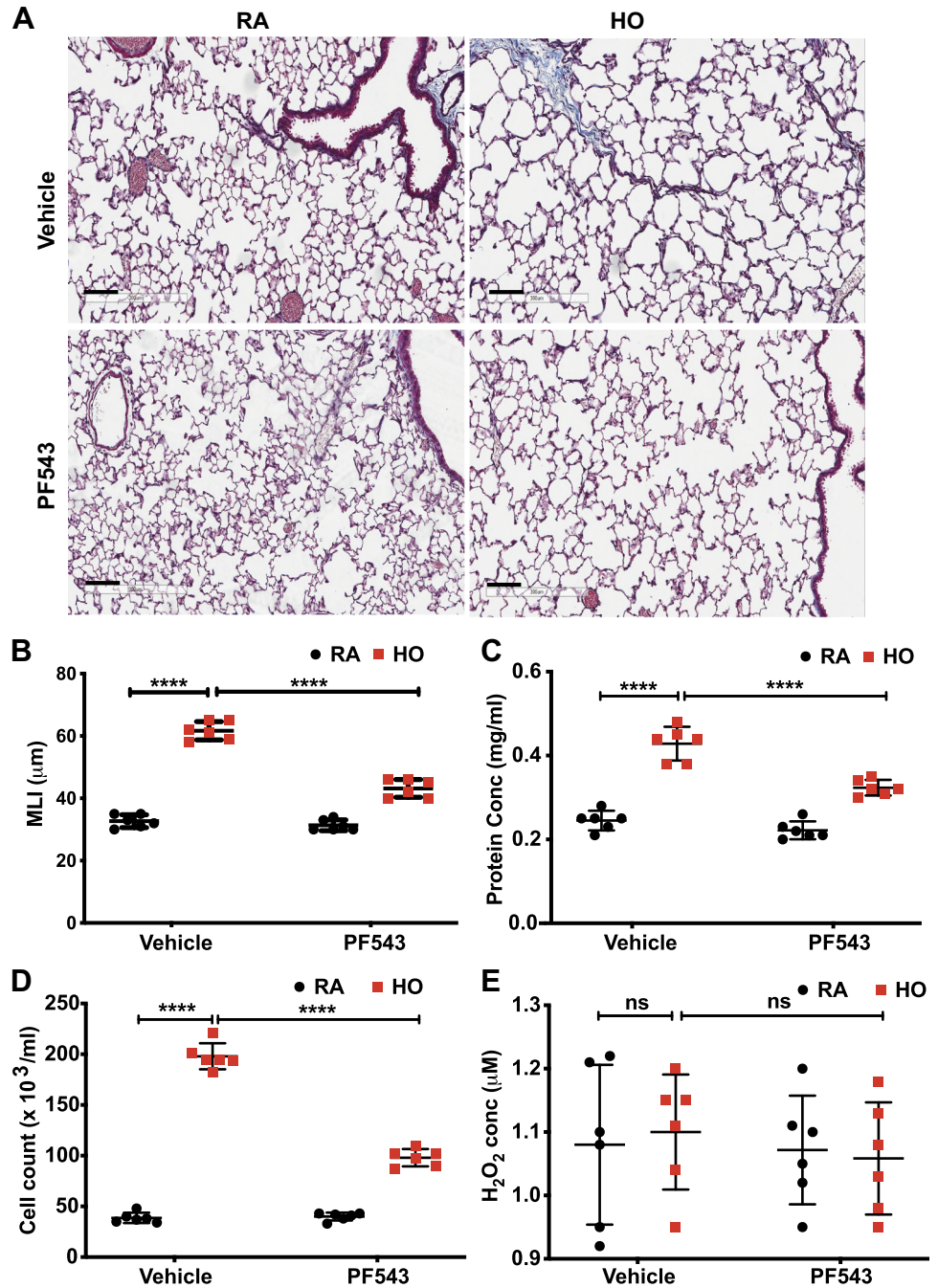
Fig. 3. Adverse effect of neonatal hyperoxia (HO) and the protective effects of PF543 last into adulthood. Neonatal mice were exposed to HO (95%) or RA and treated with PF543 or placebo. Neonatal HO led to alveolar simplification, which persisted in adults, as shown by increased mean linear intercept (MLI) compared with room air controls (*A* and *B*). The PF543-treated group which showed protection in the neonatal stage continued to grow as adults with alveolar size that is smaller compared with the HO untreated group. Neonates treated with PF543 during HO, as adults continued to show a significant decrease in bronchoalveolar lavage (BAL) total protein levels (*C*) and a decreased total cell count (*D*). Contrary to the neonatal BAL showing elevated H_2O_2 following HO exposure, there was no difference in levels of H_2O_2 among the various groups (*E*). Original view, ×10, scale bar 100 μm. Statistical analyses were done with ANOVA test. ****$P < 0.0001$, ns = not significant; $n= 6-8$/group. Equal numbers of male and female mice were used.

following exposure to HO (95%) for 7 days from PN 3 to 10 (Fig. 4*A*). We found significant AWRM when neonatal pups exposed to HO were allowed to recover in RA to become adults. Peribronchial fibrosis marked by subepithelial deposition of collagen was significantly increased in HO group (mean fibrotic area of $17.6 \pm 0.8\%$) in an area of 50 μm peripheral to the epithelial basement membrane as compared with HO treated with PF543 ($11.4 \pm 0.6\%$) (Fig. 4, *B* and *C*). PF543 treatment resulted in the normalization of these levels. There was no significant difference in peribronchial fibrosis between the RA (mean fibrotic area of $10.4 \pm 0.8\%$) and the RA group treated with PF543 (mean fibrotic area of $11.3 \pm 0.6\%$). Epithelial thickness was not increased in the airways of mice

exposed to HO compared with controls (data not shown). Goblet cell metaplasia was not significantly increased following exposure to HO (data not shown). Following neonatal exposure to HO, a 25% increase in smooth muscle layer thickness was observed (Fig. 5, *A* and *B*) that was ameliorated by neonatal treatment with PF543. There was no significant difference between the RA and the RA group treated with PF543. Airway contraction response to methacholine was assessed and evaluated as shown below.

Neonatal hyperoxia resulted in increased respiratory system resistance and airway hyperreactivity in adults, which were reduced by PF543 therapy during neonatal hyperoxia. Neonatal HO resulted in increased baseline airway resistance, as well
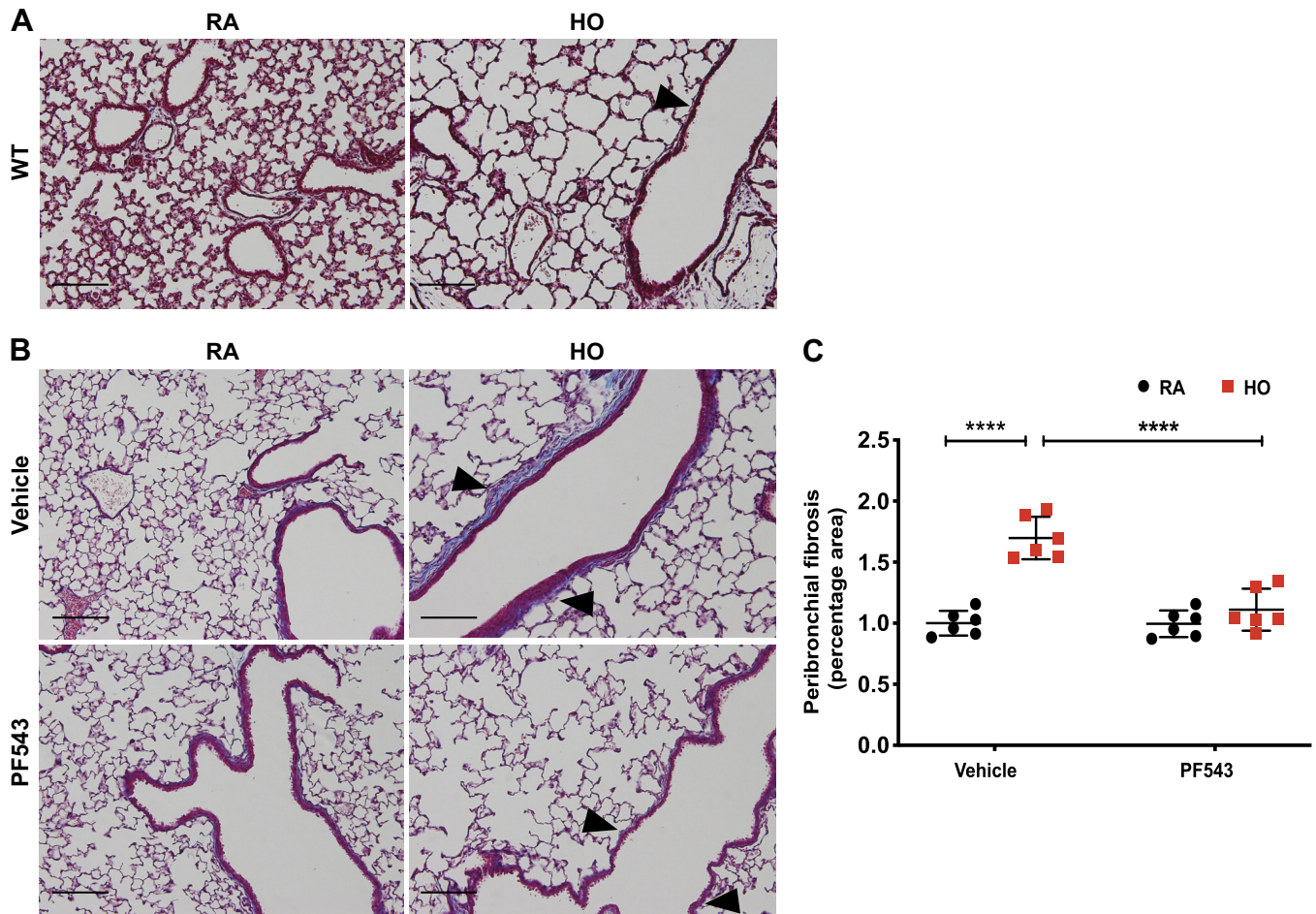
Fig. 4. PF543 therapy during neonatal hyperoxia (HO) reduced peribronchial fibrosis in adults. Neonatal mice exposed to HO did not show airway remodeling (AWRM) immediately at the end of HO. *A*: neonatal HO did not cause any peribronchial fibrosis as evidenced by absence of Masson's Trichrome staining (blue). *B*: when the HO-exposed neonatal mice were allowed to grow as adults, AWRM was noted in the form of peribronchial fibrosis. But preventive therapy with PF543 during neonatal HO ameliorated AWRM in adults. *C*: peribronchial fibrosis was quantified in Halo system using scanned lung images. The regions around the bronchi were concentrically partitioned to create a 50-μm region and area of staining measured by the Halo system. PF543 therapy significantly reduced the area of fibrosis around the bronchi. Original view, ×10, scale bar: 100 μm. Arrowheads represent peribronchial region. Fibrosis is indicated by Masson's Trichrome staining. Statistical analyses were done with ANOVA test. ****$P < 0.0001$; $n = 6$–8/group. Equal numbers of male and female mice were used.

as AHR (Fig. 6, *A* and *B*). It was interesting to note that the baseline airway resistance was elevated by 39% in HO-exposed mice treated with placebo (1.0 ± 0.04 cm $H_2O \cdot m^{-1} \cdot s^{-1}$) compared with PF543-treated and HO-exposed (0.72 ± 0.04 cm $H_2O \cdot m^{-1} \cdot s^{-1}$) and RA controls ($0.69 \pm 0.01$ cm $H_2O \cdot m^{-1} \cdot s^{-1}$). There was a significant increase in AHR to methacholine challenge in the group exposed to neonatal HO, as evidenced by an increase in progressive dose response of respiratory system resistance (R_{rs}) to methacholine (3.23 ± 0.23 cm $H_2O \cdot m^{-1} \cdot s^{-1}$) compared with RA controls (1.2 ± 0.07 cm $H_2O \cdot m^{-1} \cdot s^{-1}$). This was reduced by PF543 therapy during exposure to HO (1.2 ± 0.16 cm $H_2O \cdot m^{-1} \cdot s^{-1}$). On the basis of methacholine dose-response curves, PF543 treatment indeed resulted in significantly lower AHR. In addition, we assessed Newtonian resistance (R_n), which is a measure of central airway resistance. In commensurate with the total airway resistance, the central airway resistance was also significantly elevated in the HO group (2.18 ± 0.21 cm $H_2O \cdot m^{-1} \cdot s^{-1}$) that was significantly reduced in the PF543-treated HO group (0.8 ± 0.15 cm $H_2O \cdot m^{-1} \cdot s^{-1}$) (Fig. 6, *A* and *B*). In addition to the airway resistance, we noted adverse changes

in lung tissue impedance parameters, such as tissue resistance (*G*) and tissue elastance (*H*) (Fig. 6, *C* and *D*). In a homogeneous lung, *G* indicates the extent to which energy is dissipated in the respiratory tissue as lung volume changes, thereby indicating the resistance offered. Figure 6*D* measures lung tissue elastance, which opposes expansion of the lung (55). Tissue resistance at baseline was increased in HO-exposed lungs (10.17 ± 0.5 cm $H_2O \cdot m^{-1} \cdot s^{-1}$) compared with PF543-treated and HO-exposed (6.77 ± 0.38 cm $H_2O \cdot m^{-1} \cdot s^{-1}$) and the RA controls ($4.16 \pm 0.35$ cm$H_2O \cdot m^{-1} \cdot s^{-1}$). This was noted both at baseline and following methacholine challenge. Tissue elastance at baseline also showed a similar pattern and was increased in HO-exposed lungs (43.58 ± 6.77 cm$H_2O \cdot m^{-1} \cdot s^{-1}$) compared with PF543-treated and HO-exposed (27.13 ± 1.21 cm $H_2O \cdot m^{-1} \cdot s^{-1}$) and the RA controls ($4.16 \pm 0.35$ cm $H_2O \cdot m^{-1} \cdot s^{-1}$). This pattern was noted following methacholine challenge as well.

The luminal diameter measured was expressed as a ratio of outer diameter of the airway to the inner diameter. Commensurate with the changes seen in the airway resistance, the luminal diameter showed a reduction in HO-exposed (0.69 ± 0.03), which was improved in the HO-
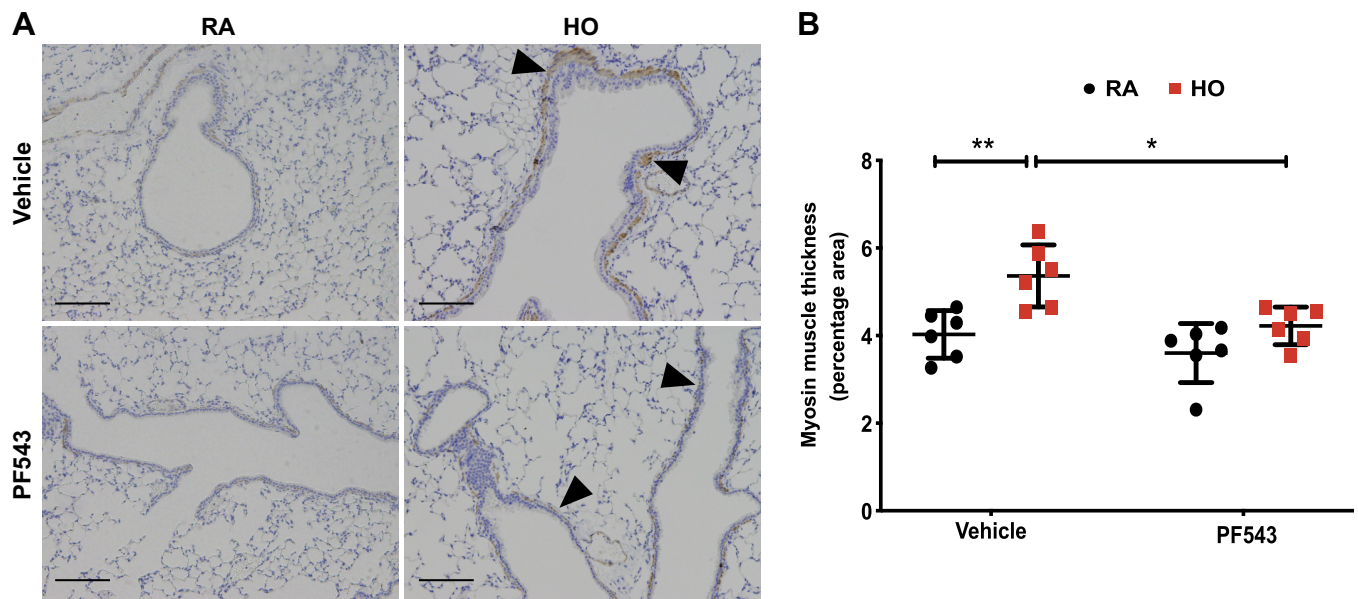
Fig. 5. PF543 therapy during neonatal hyperoxia (HO) reduced airway smooth muscle hypertrophy in adults. When the HO-exposed neonatal mice were allowed to grow as adults, airway smooth muscle thickening was noted. *A*: therapy with PF543 during neonatal HO ameliorated smooth muscle hypertrophy in adults. Paraffin-embedded lung sections were used for immunohistochemistry of myosin using smooth muscle myosin heavy chain 11 antibody. *B*: smooth muscle hypertrophy (brown) was quantified in Halo system using scanned lung images. PF543 therapy significantly reduced the area of airway smooth muscle around the bronchi. Original view, ×10; scale bar: 100 μm. Arrowheads indicate subepithelial region of airway showing smooth muscle staining. Statistical analyses were done with ANOVA test. **$P < 0.01$ and *$P \leq 0.05$; $n = 6-8$/group. Equal numbers of male and female mice were used.

exposed but PF543-treated group (0.78 ± 0.02) compared with RA controls (0.81 ± 0.02) (Fig. 6*E*).

Hyperoxia-induced reduction of epithelial cadherin (E-cadherin) in airway epithelium accompanied by elevation of SPHK1 expression in lung tissue was ameliorated by PF543. Expression of SPHK1 in the lung alveolar tissue, excluding bronchial epithelium, was assessed by immunohistochemistry followed by quantification using Halo system. Following HO as neonate, the expression of SPHK1 was significantly elevated (1.42 ± 0.1-fold) compared with RA (1.0 ± 0.05-fold). Treatment with PF543 during neonatal HO showed a tendency to reduce the impact of HO-induced increase in SPHK1 (1.18 ± 0.01-fold). PF543 therapy did not affect the expression of SPHK1 in RA (1.01 ± 0.05-fold) (Fig. 7, *A* and *B*). Expression of SPHK1 in the bronchial epithelium was similarly assessed by immunohistochemistry. Though SPHK1 was significantly present in bronchial epithelium, no significant difference was detected between the groups (data not shown).

We investigated the phenomenon of EMT as a potential mechanism underlying the development of AWRM following exposure to HO and the protective role of SPHK1 inhibition. Immediately following 7 days of HO exposure to neonates, there were no changes suggestive of AWRM (Fig. 4*A*); however, upon recovery from HO exposure and growing into adulthood, changes suggestive of AWRM were noted (Fig. 4*B*). A significant reduction in the expression of E-cadherin in adult lung airway epithelium (expressed as fold change of pixel intensity of airway epithelial layer positive for E-cadherin normalized to RA control) was evident. The intensity of E-cadherin in the HO-exposed group was reduced to 0.77 ± 0.03-fold compared with RA vehicle control group of 1.0 ± 0.02-fold (Fig. 7, *C* and *D*). This reduction in expression of E-cadherin, an epithelial marker was restored to normal levels

upon PF543 therapy (HO treated with PF543 1.13 ± 0.02-fold). Vimentin, a marker for mesenchymal transition was not elevated in the airway epithelium of the lung tissue (data not shown). Airway epithelial cells did not show any vimentin staining. Thus, we did not see changes suggestive of a complete EMT in the bronchial epithelium. The rescue of loss of E-cadherin suggested that a process of partial EMT or cytoskeletal changes triggered by neonatal HO was ameliorated following inhibition of SPHK1 by PF543. We next used human primary SAECs to study the underlying mechanism that could lead to AWRM and its amelioration by PF543 therapy.

Hyperoxia-induced E-cadherin/vimentin-related changes modulated by PF543 is associated with reduction in mtROS production in vitro. As shown in Fig. 8, *A* and *B*, a reduction in epithelial marker of E-cadherin was noted in the plasma membrane of SAECs following HO (0.17 ± 0.01-fold) compared with RA (1.0 ± 0.02-fold). PF543 therapy partially rescued the reduction in E-cadherin under HO (0.49 ± 0.01-fold). An increase in mesenchymal marker vimentin was noted following HO (8.1 ± 0.01-fold) compared with RA (1.0 ± 0.03-fold), as evidenced by its increased appearance in the cytoskeleton. This increase in vimentin under HO was also reduced by PF543 treatment (4.17 ± 0.16-fold). Quantified data are shown in Fig. 8, *B* and *D*. We noted elevated levels of H_2O_2 in the BAL of neonatal mice following exposure to HO (Fig. 2*E*) and mitochondria are considered the major cellular source of H_2O_2 (4). Hence, we investigated mitochondria as a source of ROS.

SAECs exposed to HO for 24 h showed an increased mtROS production (Fig. 8, *E* and *F*) relative to the RA control cells. This increase was ameliorated upon treatment with PF543. RA cells treated with PF543 did not show a significant difference compared with controls. The mean fluorescence intensity of
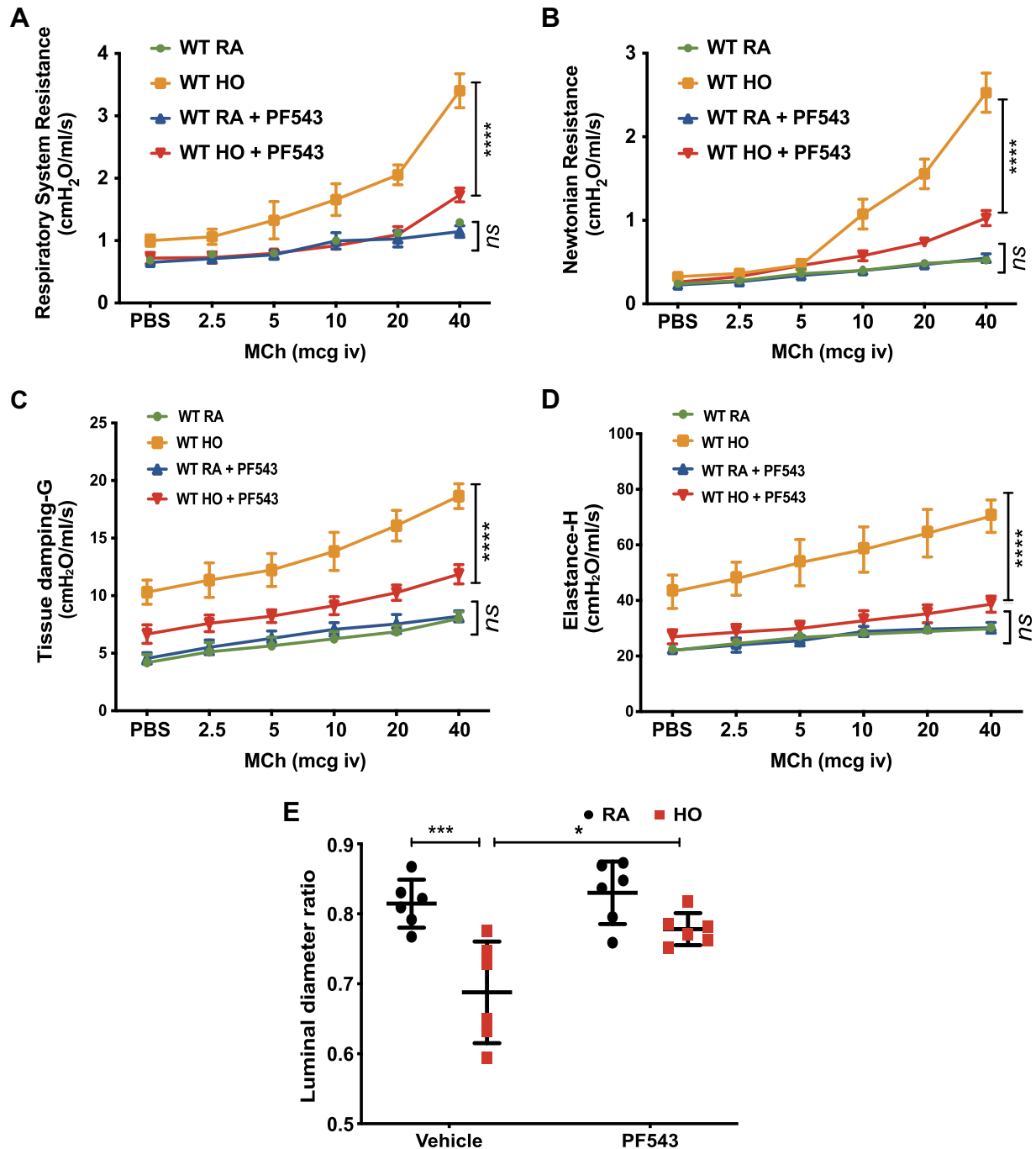
Fig. 6. PF543 therapy during neonatal hyperoxia (HO) reduced respiratory system resistance and airway hyperreactivity (AHR) in adults. HO caused an increase of both baseline respiratory system resistance (R_{rs}), as well as AHR, following methacholine (MCh) challenge. Airway constrictor hyperresponsiveness to intravenous MCh, as shown by increased respiratory system resistance (*A*) and Newtonian resistance (*B*), was measured using the Flexivent ventilator (Scireq, Tempe, AZ). Neonatal mice exposed to HO and allowed to grow to adulthood had significantly higher bronchoconstrictor responses to intravenous MCh than the neonatal mice exposed to RA. Neonatal mice exposed to HO but treated with PF543 had reduced constrictor responsiveness to methacholine challenge. Tissue impedance (*C*) was measured by tissue resistance and tissue elastance (*D*). HO-exposed mice had sustained lung tissue injury causing increased tissue impedance, which was rescued by PF543 therapy, as shown. A decrease in luminal diameter was reflective of AWRM following HO, which was rescued by PF543 therapy during HO. *E*: the ratio of luminal diameter to the outer diameter of airway was used to show airway caliber. Statistical analyses were done with ANOVA test. ****$P < 0.0001$, ***$P < 0.001$, and *$P \leq 0.05$; ns, not significant; $n = 6-8$/group. Equal numbers of male and female mice were used.

MitoSOX of the HO-treated cells, a measure of ROS, was significantly higher (1.63 ± 0.03-fold) compared with RA (1.0 ± 0.04-fold) but reduced to 1.15 ± 0.05-fold with PF543 treatment.

SPHK1 enzyme inactivation as well as inhibition reduced mtROS. In an ensuing experiment, the impact of SPHK1 in the production of mtROS was investigated. Human primary airway epithelial cells were infected with FLAG-tagged adenoviral
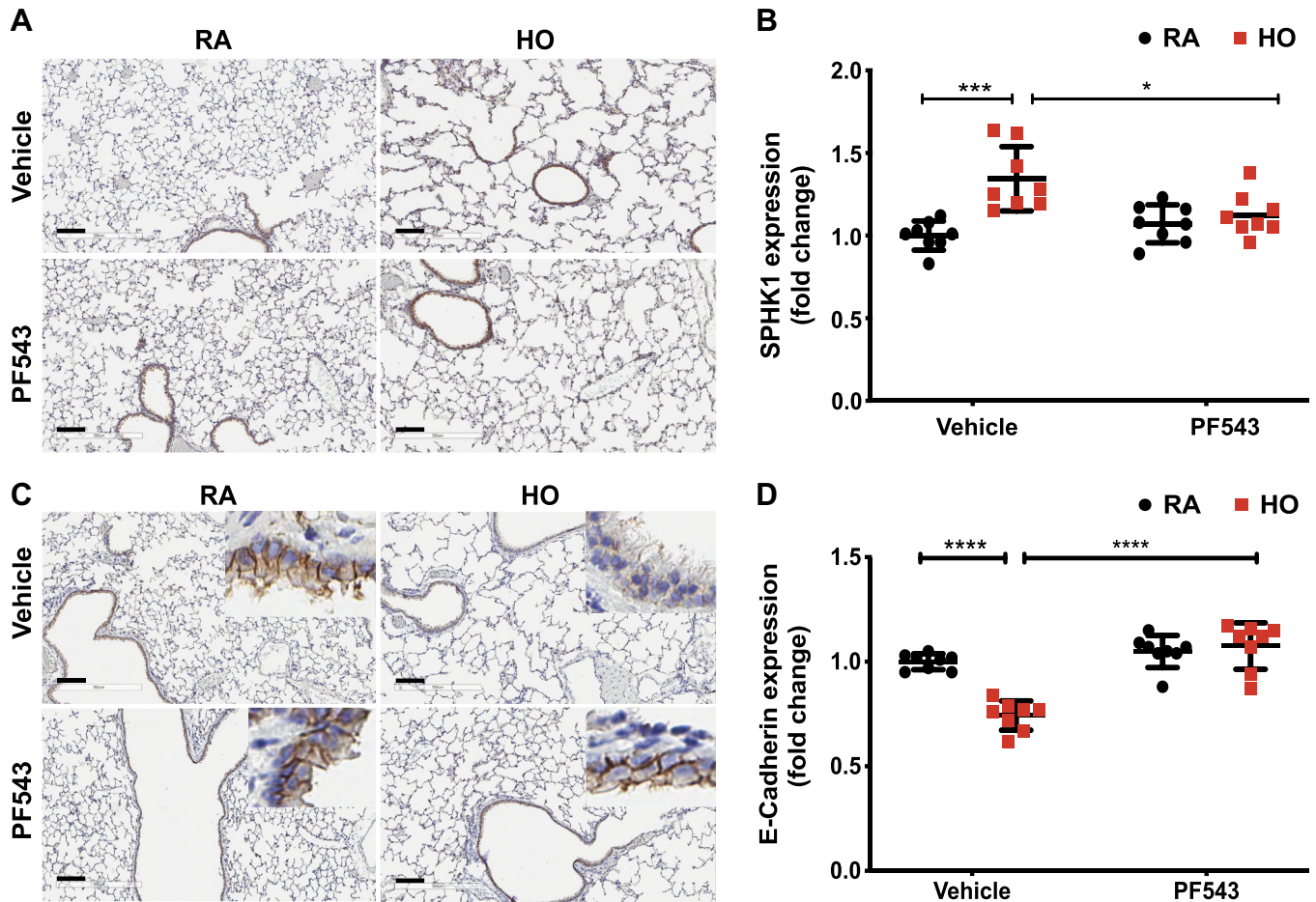
Fig. 7. PF543 therapy during neonatal hyperoxia (HO) prevented HO-induced E-cadherin reduction in bronchial airway epithelium of adult mice. As explained earlier, neonatal mice were exposed to HO (95%) from postnatal day (PN) 1–7 and lungs studied for change in expression of sphingosine kinase 1 (SPHK1) and those associated with EMT. Lung samples were stained for SPHK1 and E-cadherin, an epithelial marker. Airway epithelium did not stain for vimentin, a mesenchymal marker, even after HO (data not shown). Halo system was used to express the intensity of staining using scanned lung images. *A*: lung tissue of the HO-exposed neonatal mice showed a significant increase in expression of SPHK1 in adults. *B*: therapy with PF543 during neonatal HO ameliorated this increase in adults, as shown in the quantified data. Airway epithelium of the HO-exposed neonatal mice showed a significant reduction in expression of E-cadherin, the epithelial marker in adults (*C*). *D*: therapy with PF543 during neonatal HO prevented the reduction in adults. The epithelial lining of the bronchi was selectively partitioned and intensity of staining measured. Original view, ×10; scale bar: 100 µm. Statistical analyses were done with ANOVA test. ****$P <$ 0.0001, ***$P <$ 0.001, and *$P \leq$ 0.05; $n = 6$–8/group. Equal numbers of male and female mice were used.

Sphk1 plasmid that has a catalytically active *Sphk1* mutant (wild type) producing a functional protein and in parallel with catalytically inactive *Sphk1* plasmid. HO-induced mtROS production (2.3 ± 0.24-fold) was significantly reduced in transfected cells compared with cells infected with control vectors (1.3 ± 0.04-fold) (Fig. 9, *A* and *B*). In control cells, there was no difference between transfected and nontransfected cells in terms of ROS production, as assayed with MitoSOX. These results suggest a potential role for SPHK1 activity in mtROS formation in primary SAECs.

Scavenging of mtROS by MitoTEMPO reduced hyperoxia-induced mtROS and E-cadherin/vimentin-related changes in vitro. To further understand the role of ROS in HO-induced lung damage, we neutralized mtROS using MitoTEMPO and determined the state of partial EMT in airway epithelial cells. HO increased mtROS as evidenced by increased MitoSOX fluorescence intensity in SAECs (1.34 ± 0.5-fold) as compared with RA control (1.0 ± 0.04-fold) (Fig. 9, *C* and *D*). Treatment with MitoTEMPO significantly reduced the HO-induced Mi-

toSOX fluorescence intensity to 1.14 ± 0.03-fold. Mito-TEMPO treatment along with quenching the mtROS also reduced the expression of partial EMT markers induced by HO (Fig. 9, *E*–*H*). The fluorescence intensity of E-cadherin, which was reduced in SAECs following HO (0.18 ± 0.01-fold) was restored to normal levels after treatment with MitoTEMPO (0.36 ± 0.01-fold). Similarly, an increase in the fluorescence intensity of vimentin following HO (8.47 ± 0.29-fold) was reduced (6.9 ± 0.09-fold) by the use of MitoTEMPO. This suggests that the mtROS may play a role in HO-induced partial EMT.

DISCUSSION

Survivors of BPD suffer from pulmonary sequelae, such as wheezing, frequent pneumonia, pulmonary hypertension, early adult emphysema, and early decline in adult lung function. Multiple insults including HO and ventilator-induced injury result in inflammation of the neonatal lung, causing aberrant
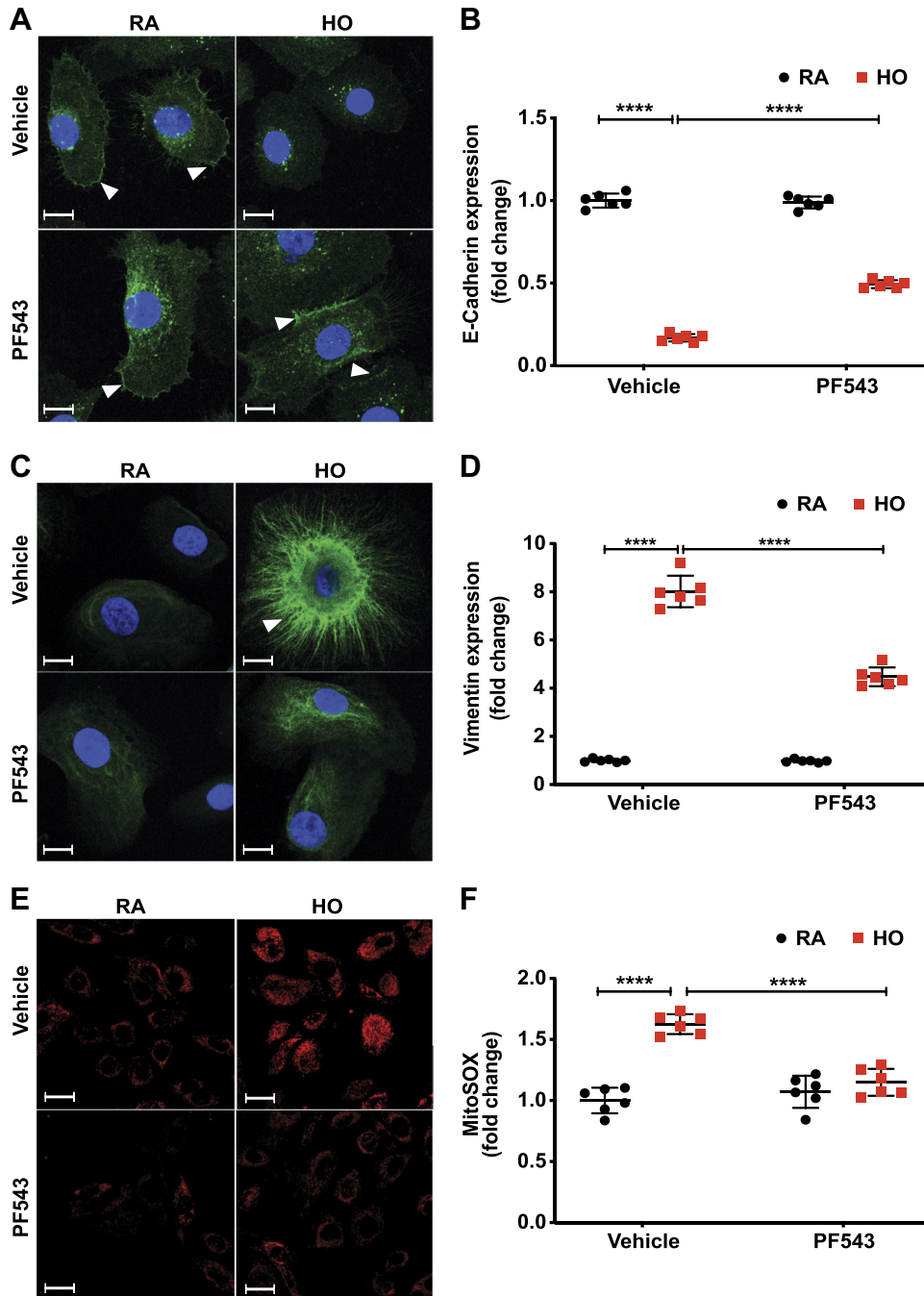
Fig. 8. Sphingosine kinase 1 (SPHK1) inhibitor, PF543, attenuates hyperoxia (HO)- induced epithelial-mesenchymal transition (EMT) in human primary small airway epithelial cells (SAECs) associated with reduced mitochondrial ROS (mtROS). *A*: E-cadherin staining of cell periphery was detected by immunofluorescence staining. PF543 inhibited HO-induced degradation of E-cadherin at the cell periphery. Shown is a representative image from several experiments. *B*: following HO, there was a significant reduction in expression of E-cadherin in cell periphery, which was restored by treatment with PF543. No difference was noted between the two groups treated with RA and pretreated with or without PF543. *C*: PF543 inhibited the HO-induced increase in the vimentin cytoskeleton, as seen in cells exposed to HO. *D*: following HO, there was a significant increase in expression of vimentin cytoskeleton, which was reduced by treatment with PF543. *E*: no difference was noted between the two groups treated with room air (RA) and pretreated with or without PF543. Three hours of exposure was used for experiments to detect mtROS using MitoSOX. PF543 inhibited HO-induced increase in mtROS compared with cells exposed to RA. *E*: representative image from several experiments. *F*: following HO, there was a significant increase in expression of mtROS, which was reduced by treatment with PF543. No difference was noted between the two groups treated with RA and pretreated with or without PF543. IgG and secondary antibody-only controls were used. Original view, ×60; scale bar: 20 μm. Statistical analyses were done with ANOVA test. ****$P < 0.0001$. Images for control and treatment groups in microscopy experiments were collected at the same time under the same conditions.

lung development (50). Here, we have unraveled the protective role of the SPHK1 inhibitor, PF543, in the prevention of BPD in the developing lung followed by tempering of the long-term sequela of wheezing due to AWRM.

Elevated levels of S1P have been shown in patients with asthma and idiopathic pulmonary fibrosis (27, 39, 48). S1P is known to play varied roles in the pathogenesis of asthma, including AWRM (17, 30). The significance of sphingolipids in neonatal lung disease has been brought to light only within the last decade (22, 56). Hendricks-Muñoz et al. (23) have shown that S1P is elevated in the tracheal aspirates of neonatal infants with BPD and, hence, could serve as a biomarker of BPD. Similarly, in our study, we have noted an increase of S1P

level in tracheal aspirates of patients with severe BPD. Dihydro-S1P was also detected in tracheal aspirates of infants born preterm, irrespective of BPD. However, it was not detected in the tracheal aspirates of term infants (Table 1). S1P and dihydro-S1P levels are upregulated both in human idiopathic pulmonary fibrosis (IPF) and animal models of pulmonary fibrosis (Fig. 10)(27). Dihydro-S1P is structurally similar to S1P and could serve as a potent sphingophospholipid mediator; however, its significance in lung pathology is not known, although it has been shown to play an antifibrotic role in systemic sclerosis (6, 40).

A pathological role for S1P in the development of BPD was noted in our earlier study using a murine model of HO. HO

Fig. 9. Inactivation of sphingosine kinase 1 (SPHK1) by mutant enzyme is associated with reduced mitochondrial reactive oxygen species (mtROS) formation. MitoTEMPO inhibited mtROS formation accompanied by reduced epithelial-mesenchymal transition (EMT). Human primary airway epithelial cells were infected with SPHK1 mutant, as well as with catalytically inactive FLAG-tagged adenoviral *Sphk1* plasmid. Hyperoxia (HO)-induced mtROS production was significantly reduced in transfected cells compared with cells infected with control vectors (*A* and *B*; **$P \leq 0.01$). *C*: in control cells, there was no difference in MitoSOX between transfected and nontransfected cells. MitoTEMPO inhibited HO-induced increase in mtROS compared with cells exposed to room air (RA). Shown is a representative image from several experiments. *D*: following HO, there was a significant increase in expression of mtROS, which was reduced by treatment with MitoTEMPO. No difference was noted between the two groups treated with RA and pretreated with or without MitoTEMPO. E-cadherin staining of cell periphery was detected by immunofluorescence staining. *E*: MitoTEMPO inhibited HO-induced degradation of E-cadherin at cell periphery compared with cells exposed to RA. *F*: following hyperoxia, there was a significant reduction in expression of E-cadherin in cell periphery, which was restored by treatment with MitoTEMPO. No difference was noted between the two groups treated with RA and pretreated with or without MitoTEMPO. *G*: MitoTEMPO inhibited HO-induced increase of the vimentin cytoskeleton compared with cells exposed to RA. *H*: following HO, there was a significant increase in expression of the vimentin cytoskeleton, which was reduced by treatment with MitoTEMPO. No difference was noted between the two groups treated with RA and pretreated with or without PF543. IgG and secondary antibody-only controls were used. Original view, ×10; scale bar: 20 μm. Statistical analyses were done with ANOVA test. ****$P < 0.0001$, *$P \leq 0.05$. Images for control and treatment groups in microscopy experiments were collected at the same time under the same conditions.
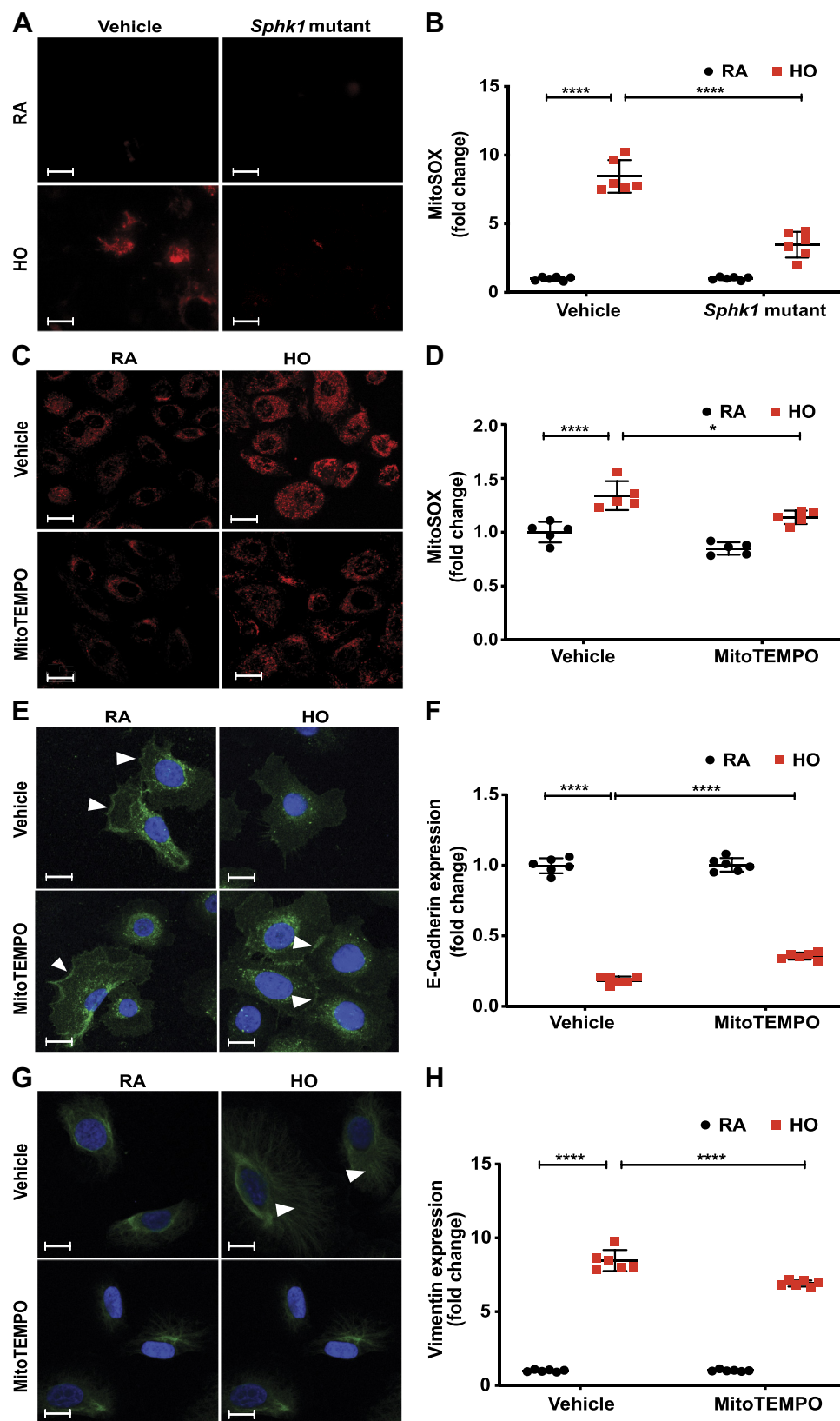
increased the expression of SPHK1 in the lung tissue, followed by an increase of S1P. *Sphk1*$^{-/-}$ mice showed protection against HO-induced neonatal BPD (22). S1P plays an active role in the generation of ROS (35), and inhibition of SPHK1 by PF543 in in vitro experiments reduced ROS formation (21). In the current study, we used PF543 to inhibit SPHK1 during neonatal exposure to HO in the murine model of BPD. PF543 therapy improved alveolarization (Fig. 2), ameliorating BPD.

ROOM AIR

HYPEROXIA

HYPEROXIA + PF543

Increased SPHK1, S1P and ROS

SPHK1 inhibition: Reduced Mitochondrial ROS

Reduced Airway Epithelial E-cadherin (partial EMT)

Retained Airway Epithelial E-cadherin (reduced partial EMT)

Normal Airway with no AWRM

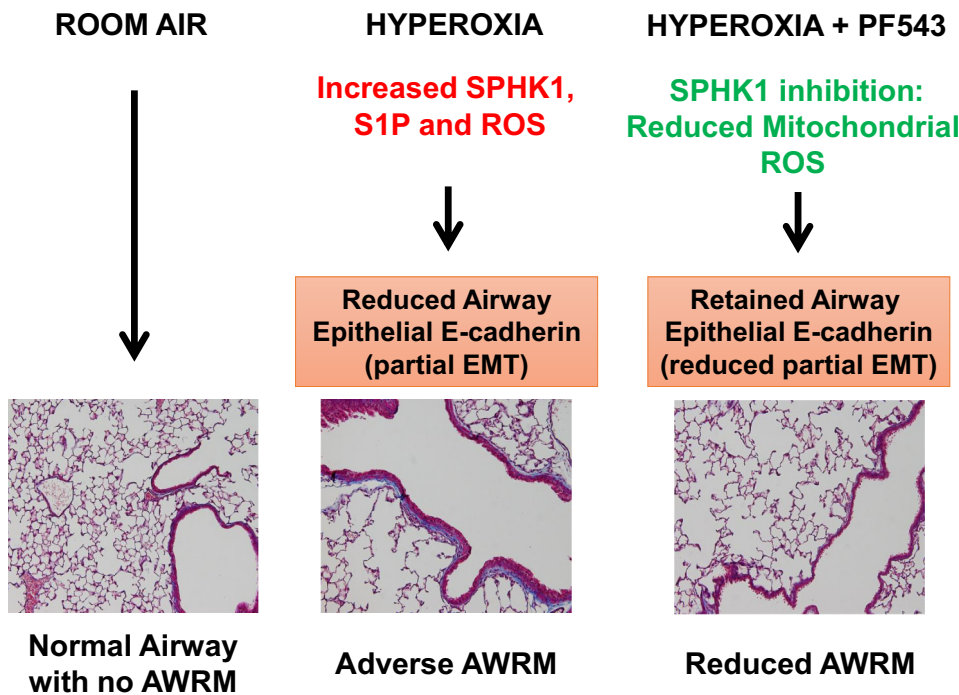**Adverse AWRM**

Reduced AWRM

Fig. 10. Schema showing the summary of role of sphingolipids in hyperoxia (HO)-induced neonatal lung injury. HO causes an increase in sphingosine kinase 1 (SPHK1), which stimulates the formation of sphingosine 1-phosphate (S1P). HO leads to increased formation of reactive oxygen species (ROS), including mitochondrial (mt)ROS, leading to reduction in airway epithelial E-cadherin (partial EMT) associated with adverse airway remodeling (AWRM). Inhibition of SPHK1 by PF543 was associated with reduced ROS formation and inhibition of mtROS. This was associated with restoration of epithelial E-cadherin [reduced partial epithelial-mesenchymal transition (EMT)], probably leading to reduced AWRM.

We also noted reduced formation of ROS (H_2O_2) in BAL. This was the immediate impact of PF543 therapy.

Wheezing and AHR have been reported in survivors of BPD who require prolonged oxygen treatment (7, 58, 59). Wheezing, as a sequela of BPD, is shown to be unrelated to atopy, as there is no increased incidence of atopy reported in BPD patients (37, 52). AWRM contributes to fixed airway obstruction and AHR. This could manifest as wheezing resistant to albuterol therapy (41, 43). Autopsy findings of airways from babies who had BPD showed a significant airway wall thickening involving the layers of epithelium, subepithelium, and smooth muscle (1, 38, 57). This finding has also been reported in CT scans of BPD survivors (46). In our study, neonatal mice exposed to HO, upon growing up as adults, showed increased subepithelial/peribronchial fibrosis and thickening of smooth muscle layer similar to an earlier report by Royce et al. (49). These findings in animal models are consistent with the features seen in human BPD and have been reported by other investigators as well (32, 33). The increase in smooth muscle thickness, though statistically significant, was only ~25% (Fig. 5). Following neonatal HO, O'Reilly et al. (14) have reported resolution of airway smooth muscle hypertrophy upon room air recovery by 8 wk of age.

We have earlier shown in our murine model that HO caused an increase in SPHK1 expression accompanied by an increase in S1P concentration (21, 22). PF543 therapy caused a significant reduction in plasma S1P concentration (Fig. 2G). In this study, HO exposure of neonatal pups was associated with an increase in expression of SPHK1 in the alveolar component of lung tissue on PN 56 in adult mice. No significant increase was noted in the bronchial epithelium. Interestingly, inhibition of SPHK1 activity with PF543 during neonatal exposure was associated with a reduced expression of SPHK1 in adult mice. It is possible that ROS generated following neonatal HO triggered an upregulation of SPHK1 in lung tissue, which

persisted into adulthood, resulting in damage over a long period of time. The mechanism by which neonatal HO leads to persistent increase of SPHK1 expression in adult mice is of great interest and merits further investigation.

SPHK1 inhibition with PF543 during exposure of neonatal mice pups to HO reduced AWRM as well as AHR compared with vehicle-treated HO controls. BAL analysis in adult mice exposed to HO as neonates did not show any significant difference in the levels of ROS (H_2O_2) but had increased markers of inflammation (Fig. 3). PF543-treated group, exposed to HO, had reduced AWRM in line with reduced AHR. This rescue phenomenon has not been previously reported in BPD. In asthma, an earlier generation SPHK1 inhibitor, SKI-II, inhibited antigen-dependent activation of human and murine mast cells and significantly reduced OVA-induced AHR to methacholine (44, 47). This was accompanied by decreased pulmonary inflammation. In our experiment, it was noted that the impact of neonatal PF543 therapy during HO lasted long, reducing both AWRM and AHR in adults. Beyond the large airways, an increase in G following HO is suggestive of functional consequences of increased lung tissue resistance, inclusive of that offered by peripheral airways. Therapy at the neonatal stage during HO exposure has protective effects in the lung tissue that correlates well with alveolar protection noted. A significant increase in H in the HO-exposed group, even at the baseline, is suggestive of the damage to lung tissue, as it offers greater resistance to expansion. This finding highlights the importance of preventing long-term damage during the critical stages of lung development to have improved lung function throughout life. Mice have larger airways in relation to lung size and less airway generations when compared with human lungs (10). Hence, caution must be exercised in the interpretation of the data as HO-induced airway remodeling could have differential effects on the lung mechanics between humans and mice.

Investigating into the mechanisms that could lead to AWRM, we focused on airway epithelial injury. By using immunohistochemical staining of lung tissue, we were able to differentially study the expression of proteins in bronchial epithelium and the rest of lung parenchyma. The bronchial epithelium was shown to be particularly vulnerable to the effects of airborne oxidative stress, as these cells are in direct contact with the environment (15, 18). Cross talk between the epithelium and the underlying mesenchyme was shown to drive AWRM in asthma and idiopathic pulmonary fibrosis (12, 25). EMT is one of the factors driving injured epithelial cell to undergo mesenchymal changes, triggering events leading to peribronchial fibrosis and AWRM (24). EMT is a biological process where epithelial cells lose adhesion and acquire mesenchymal traits with increased motility, migration, and enhanced production of extracellular matrix proteins (20). SPHK1 expression was upregulated in lung tissue from patients with IPF, which correlated well with increased EMT markers and decline in lung function (26, 39). We investigated the possibility of a similar phenomenon in HO-induced BPD. S1P is known to induce EMT, which could trigger peribronchial fibrosis, leading to AWRM, as has been noted in idiopathic pulmonary fibrosis (36, 39). We did not see any evidence of a complete EMT in bronchial airway epithelium, as we noted only a reduction in adherens junction protein E-cadherin without an accompanying increase in vimentin. This may be considered as incomplete or partial EMT. The EMT-related changes such as a reduction in E-cadherin and an increase in vimentin noted in our study following HO were reversed by SPHK1 inhibition using PF543 in only in vitro cell lines but not in the in vivo animal model.

Both S1P and ROS are known inducers of EMT (9, 61, 62). There were no changes suggestive of AWRM in the immediate aftermath of neonatal HO but became evident in adult mice (Fig. 4). Although we did not see changes suggestive of complete EMT, bronchial epithelial reduction of expression of E-cadherin was evident in the lung tissue of adult mice exposed to HO as neonates, showing AWRM (Fig. 7). This was ameliorated by PF543 therapy during neonatal HO, which was associated with reduced ROS levels in BAL. This suggested that the neonatal insult triggered the pathological process, leading to AWRM later in life.

To study AWRM, we used human primary small airway epithelial cells. We investigated the role of mtROS, as mitochondria is considered the primary source of superoxide that gets converted to H_2O_2, which was significantly elevated in the BAL of neonatal mice, following HO. It has been recently published that in the absence of SPHK1, the mitochondrial accumulation of ROS was significantly reduced in acetaminophen-treated hepatocytes (34). In another recent study, blocking SPHK1 activity with PF543 attenuated TGF-β-induced expression of fibronectin and α-smooth muscle actin by reduced mtROS, suggesting a link between SPHK1/S1P and mitochondria in fibroblast activation (28). We noted that HO-induced mtROS production was suppressed by inactivation or inhibition of SPHK1. We notice a striking difference between the in vivo and in vitro models characterized by what could be described as a partial EMT seen in vivo, in contrast to a more complete EMT-like change seen in vitro. This disparity noted by us has already been reported in the literature in the context of cancer (5). This led to the classification of loss of E-cadherin

unaccompanied by an increase of vimentin as partial EMT and got named as "actin diseases." This could be the phenomenon seen in hyperoxia-induced AWRM in BPD, which is different from classic EMT of embryonic development or what is seen in vitro. This is the first report of inhibition of SPHK1 using PF543 leading to reduced mtROS in airway epithelial cells that was associated with reduced E-cadherin, the critical cell adhesion molecule. Independent of SPHK1 inhibition, scavenging of mtROS by MitoTEMPO also reduced E-cadherin/vimentin-related changes in vitro. On the basis of our experimental findings, we suggest that AWRM in BPD following HO could be triggered by changes suggestive of partial-EMT or reduced E-cadherin in bronchial epithelial cells, induced by mtROS, mediated by SPHK1.

Conclusion. Inhibition of SPHK1 with PF543 during neonatal HO exposure inhibited ROS formation in the lungs, an immediate or short-term effect. The long-term consequences were also mitigated, as reflected in reduced AWRM and AHR in adult lungs in the murine model. From a therapeutic point of view, the protective effect of SPHK1 inhibition in BPD and its sequela of AWRM could be related to inhibition of mtROS during HO triggering partial EMT-like changes. Inhibition of SPHK1 during the HO insult resulted in reduction of partial EMT-like changes preventing AWRM. These findings have significant therapeutic potential to a problem as intractable as BPD and its sequela of wheezing.

DISCLAIMERS

No role was played by the funding body in the design of the study, collection, analysis and interpretation of data or in writing the manuscript.

DISCLOSURES

No conflicts of interest, financial or otherwise, are declared by the authors.

AUTHOR CONTRIBUTIONS

A.W.H., T.S., D.L.E., S.J.A., V.N., and A.H. conceived and designed research; A.W.H., T.S., D.L.E., P.F., and A.H. performed experiments; A.W.H., T.S., D.L.E., P.F., E.V.B., and A.H. analyzed data; A.W.H., T.S., D.L.E., P.F., E.V.B., S.J.A., V.N., and A.H. interpreted results of experiments; A.W.H., T.S., D.L.E., and P.F. prepared figures; A.H. drafted manuscript; A.W.H., T.S., E.V.B., S.J.A., V.N., and A.H. edited and revised manuscript; A.W.H., T.S., D.L.E., P.F., E.V.B., S.J.A., V.N., and A.H. approved final version of manuscript.

REFERENCES

1. **Abman SH, Bancalari E, Jobe A.** The evolution of bronchopulmonary dysplasia after 50 years. *Am J Respir Crit Care Med* 195: 421–424, 2017. doi:10.1164/rccm.201611-2386ED.

2. **Ammit AJ, Hastie AT, Edsall LC, Hoffman RK, Amrani Y, Krymskaya VP, Kane SA, Peters SP, Penn RB, Spiegel S, Panettieri RA Jr.** Sphingosine 1-phosphate modulates human airway smooth muscle cell functions that promote inflammation and airway remodeling in asthma. *FASEB J* 15: 1212–1214, 2001. doi:10.1096/fj.00-0742fje.

3. **Barker DJ.** Fetal origins of coronary heart disease. *BMJ* 311: 171–174, 1995. doi:10.1136/bmj.311.6998.171.

4. **Bolisetty S, Jaimes EA.** Mitochondria and reactive oxygen species: physiology and pathophysiology. *Int J Mol Sci* 14: 6306–6344, 2013. doi:10.3390/ijms14036306.

5. **Bruner HC, Derksen PWB.** Loss of E-cadherin-dependent cell-cell adhesion and the development and progression of cancer. *Cold Spring Harb Perspect Biol* 10: a029330, 2018. doi:10.1101/cshperspect.a029330.

6. **Bu S, Asano Y, Bujor A, Highland K, Hant F, Trojanowska M.** Dihydrosphingosine 1-phosphate has a potent antifibrotic effect in scleroderma fibroblasts via normalization of phosphatase and tensin homolog levels. *Arthritis Rheum* 62: 2117–2126, 2010. doi:10.1002/art.27463.

7. **Caskey S, Gough A, Rowan S, Gillespie S, Clarke J, Riley M, Megarry J, Nicholls P, Patterson C, Halliday HL, Shields MD, McGarvey L.** Structural and functional lung impairment in adult survivors of bronchopulmonary dysplasia. *Ann Am Thorac Soc* 13: 1262–1270, 2016. doi:10.1513/AnnalsATS.201509-578OC.

8. **Chen B, Moore TV, Li Z, Sperling AI, Zhang C, Andrade J, Rodriguez A, Bahroos N, Huang Y, Morrisey EE, Gruber PJ, Solway J.** Gata5 deficiency causes airway constrictor hyperresponsiveness in mice. *Am J Respir Cell Mol Biol* 50: 787–795, 2014. doi:10.1165/rcmb.2013-0294OC.

9. **Cichon MA, Radisky DC.** ROS-induced epithelial-mesenchymal transition in mammary epithelial cells is mediated by NF-κB-dependent activation of Snail. *Oncotarget* 5: 2827–2838, 2014. doi:10.18632/oncotarget.1940.

10. **Counter WB, Wang IQ, Farncombe TH, Labiris NR.** Airway and pulmonary vascular measurements using contrast-enhanced micro-CT in rodents. *Am J Physiol Lung Cell Mol Physiol* 304: L831–L843, 2013. doi:10.1152/ajplung.00281.2012.

11. **Daniels SR.** The Barker hypothesis revisited. *J Pediatr* 173: 1–3, 2016. doi:10.1016/j.jpeds.2016.04.031.

12. **Davies DE.** The role of the epithelium in airway remodeling in asthma. *Proc Am Thorac Soc* 6: 678–682, 2009. doi:10.1513/pats.200907-067DP.

13. **Doyle LW, Anderson PJ.** Long-term outcomes of bronchopulmonary dysplasia. *Semin Fetal Neonatal Med* 14: 391–395, 2009. doi:10.1016/j.siny.2009.08.004.

14. **Dylag AM, Haak J, Yee M, O'Reilly MA.** Pulmonary mechanics and structural lung development after neonatal hyperoxia in mice. *Pediatr Res* 87: 1201–1210, 2020. doi:10.1038/s41390-019-0723-y.

15. **Erzurum SC, Danel C, Gillissen A, Chu CS, Trapnell BC, Crystal RG.** In vivo antioxidant gene expression in human airway epithelium of normal individuals exposed to 100% O₂. *J Appl Physiol (1985)* 75: 1256–1262, 1993. doi:10.1152/jappl.1993.75.3.1256.

16. **Fakhoury KF, Sellers C, Smith EO, Rama JA, Fan LL.** Serial measurements of lung function in a cohort of young children with bronchopulmonary dysplasia. *Pediatrics* 125: e1441–e1447, 2010. doi:10.1542/peds.2009-0668.

17. **Fuerst E, Foster HR, Ward JP, Corrigan CJ, Cousins DJ, Woszczek G.** Sphingosine-1-phosphate induces pro-remodelling response in airway smooth muscle cells. *Allergy* 69: 1531–1539, 2014. doi:10.1111/all.12489.

18. **Gao W, Li L, Wang Y, Zhang S, Adcock IM, Barnes PJ, Huang M, Yao X.** Bronchial epithelial cells: The key effector cells in the pathogenesis of chronic obstructive pulmonary disease? *Respirology* 20: 722–729, 2015. doi:10.1111/resp.12542.

19. **Greenough A, Dimitriou G, Bhat RY, Broughton S, Hannam S, Rafferty GF, Leipälä JA.** Lung volumes in infants who had mild to moderate bronchopulmonary dysplasia. *Eur J Pediatr* 164: 583–586, 2005. doi:10.1007/s00431-005-1706-z.

20. **Guida G, Riccio AM.** Immune induction of airway remodeling. *Semin Immunol* 46: 101346, 2019. doi:10.1016/j.smim.2019.101346.

21. **Harijith A, Pendyala S, Ebenezer DL, Ha AW, Fu P, Wang YT, Ma K, Toth PT, Berdyshev EV, Kanteti P, Natarajan V.** Hyperoxia-induced p47phox activation and ROS generation is mediated through S1P transporter Spns2, and S1P/S1P1&2 signaling axis in lung endothelium. *Am J Physiol Lung Cell Mol Physiol* 311: L337–L351, 2016. doi:10.1152/ajplung.00447.2015.

22. **Harijith A, Pendyala S, Reddy NM, Bai T, Usatyuk PV, Berdyshev E, Gorshkova I, Huang LS, Mohan V, Garzon S, Kanteti P, Reddy SP, Raj JU, Natarajan V.** Sphingosine kinase 1 deficiency confers protection against hyperoxia-induced bronchopulmonary dysplasia in a murine model: role of S1P signaling and Nox proteins. *Am J Pathol* 183: 1169–1182, 2013. doi:10.1016/j.ajpath.2013.06.018.

23. **Hendricks-Muñoz KD, Xu J, Voynow JA.** Tracheal aspirate VEGF and sphingolipid metabolites in the preterm infant with later development of bronchopulmonary dysplasia. *Pediatr Pulmonol* 53: 1046–1052, 2018. doi:10.1002/ppul.24022.

24. **Holgate ST, Davies DE, Lackie PM, Wilson SJ, Puddicombe SM, Lordan JL.** Epithelial-mesenchymal interactions in the pathogenesis of asthma. *J Allergy Clin Immunol* 105: 193–204, 2000. doi:10.1016/S0091-6749(00)90066-6.

25. **Horowitz JC, Thannickal VJ.** Epithelial-mesenchymal interactions in pulmonary fibrosis. *Semin Respir Crit Care Med* 27: 600–612, 2006. doi:10.1055/s-2006-957332.

26. **Huang LS, Berdyshev E, Mathew B, Fu P, Gorshkova IA, He D, Ma W, Noth I, Ma SF, Pendyala S, Reddy SP, Zhou T, Zhang W, Garzon SA, Garcia JG, Natarajan V.** Targeting sphingosine kinase 1 attenuates bleomycin-induced pulmonary fibrosis. *FASEB J* 27: 1749–1760, 2013. doi:10.1096/fj.12-219634.

27. **Huang LS, Natarajan V.** Sphingolipids in pulmonary fibrosis. *Adv Biol Regul* 57: 55–63, 2015. doi:10.1016/j.jbior.2014.09.008.

28. **Huang LS, Sudhadevi T, Fu P, Punathil-Kannan PK, Ebenezer DL, Ramchandran R, Putherickal V, Cheresh P, Zhou G, Ha AW, Harijith A, Kamp DW, Natarajan V.** Sphingosine kinase 1/S1P signaling contributes to pulmonary fibrosis by activating hippo/YAP pathway and mitochondrial reactive oxygen species in lung fibroblasts. *Int J Mol Sci* 21: 2064, 2020. doi:10.3390/ijms21062064.

29. **Jobe AH, Bancalari E.** Bronchopulmonary dysplasia. *Am J Respir Crit Care Med* 163: 1723–1729, 2001. doi:10.1164/ajrccm.163.7.2011060.

30. **Karmouty-Quintana H, Siddiqui S, Hassan M, Tsuchiya K, Risse PA, Xicota-Vila L, Marti-Solano M, Martin JG.** Treatment with a sphingosine-1-phosphate analog inhibits airway remodeling following repeated allergen exposure. *Am J Physiol Lung Cell Mol Physiol* 302: L736–L745, 2012. doi:10.1152/ajplung.00050.2011.

31. **Kennedy KA, Cotten CM, Watterberg KL, Carlo WA.** Prevention and management of bronchopulmonary dysplasia: Lessons learned from the neonatal research network. *Semin Perinatol* 40: 348–355, 2016. doi:10.1053/j.semperi.2016.05.010.

32. **Kumar VH, Lakshminrusimha S, Kishkurno S, Paturi BS, Gugino SF, Nielsen L, Wang H, Ryan RM.** Neonatal hyperoxia increases airway reactivity and inflammation in adult mice. *Pediatr Pulmonol* 51: 1131–1141, 2016. doi:10.1002/ppul.23430.

33. **Kumar VHS, Wang H, Kishkurno S, Paturi BS, Nielsen L, Ryan RM.** Long-term effects of neonatal hyperoxia in adult mice. *Anat Rec (Hoboken)* 301: 717–726, 2018. doi:10.1002/ar.23766.

34. **Li L, Wang H, Zhang J, Sha Y, Wu F, Wen S, He L, Sheng L, You Q, Shi M, Liu L, Zhou H.** SPHK1 deficiency protects mice from acetaminophen-induced ER stress and mitochondrial permeability transition. *Cell Death Differ* 27: 1924–1937, 2020. doi:10.1038/s41418-019-0471-x.

35. **Lin CC, Yang CC, Cho RL, Wang CY, Hsiao LD, Yang CM.** Sphingosine 1-phosphate-induced ICAM-1 expression via NADPH oxidase/ROS-dependent NF-κB cascade on human pulmonary alveolar epithelial cells. *Front Pharmacol* 7: 80, 2016. doi:10.3389/fphar.2016.00080.

36. **Liu H, Ma Y, He HW, Zhao WL, Shao RG.** SPHK1 (sphingosine kinase 1) induces epithelial-mesenchymal transition by promoting the autophagy-linked lysosomal degradation of CDH1/E-cadherin in hepatoma cells. *Autophagy* 13: 900–913, 2017. doi:10.1080/15548627.2017.1291479.

37. **Lum S, Kirkby J, Welsh L, Marlow N, Hennessy E, Stocks J.** Nature and severity of lung function abnormalities in extremely pre-term children at 11 years of age. *Eur Respir J* 37: 1199–1207, 2011. doi:10.1183/09031936.00071110.

38. **Margraf LR, Tomashefski JF Jr, Bruce MC, Dahms BB.** Morphometric analysis of the lung in bronchopulmonary dysplasia. *Am Rev Respir Dis* 143: 391–400, 1991. doi:10.1164/ajrccm/143.2.391.

39. **Milara J, Navarro R, Juan G, Peiró T, Serrano A, Ramón M, Morcillo E, Cortijo J.** Sphingosine-1-phosphate is increased in patients with idiopathic pulmonary fibrosis and mediates epithelial to mesenchymal transition. *Thorax* 67: 147–156, 2012. doi:10.1136/thoraxjnl-2011-200026.

40. **Mishima Y, Kurano M, Kobayashi T, Nishikawa M, Ohkawa R, Tozuka M, Yatomi Y.** Dihydro-sphingosine 1-phosphate interacts with carrier proteins in a manner distinct from that of sphingosine 1-phosphate. *Biosci Rep* 38: BSR20181288, 2018. doi:10.1042/BSR20181288.

41. **Morrow DK, Schilling D, McEvoy CT.** Response to bronchodilators in very preterm infants with evolving bronchopulmonary dysplasia. *Res Rep Neonatol* 5: 113–117, 2015. doi:10.2147/RRN.S96961.

42. **Nardiello C, Mižíková I, Silva DM, Ruiz-Camp J, Mayer K, Vadász I, Herold S, Seeger W, Morty RE.** Standardisation of oxygen exposure in the development of mouse models for bronchopulmonary dysplasia. *Dis Model Mech* 10: 185–196, 2017. doi:10.1242/dmm.027086.

43. **Ng G, da Silva O, Ohlsson A.** Bronchodilators for the prevention and treatment of chronic lung disease in preterm infants. *Cochrane Database Syst Rev* 12: CD003214, 2016. doi:10.1002/14651858.CD003214.pub3.

44. **Nishiuma T, Nishimura Y, Okada T, Kuramoto E, Kotani Y, Jahangeer S, Nakamura S.** Inhalation of sphingosine kinase inhibitor attenuates airway inflammation in asthmatic mouse model. *Am J Physiol Lung Cell Mol Physiol* 294: L1085–L1093, 2008. doi:10.1152/ajplung.00445.2007.

45. **O'Reilly M, Sozo F, Harding R.** Impact of preterm birth and bronchopulmonary dysplasia on the developing lung: long-term consequences for respiratory health. *Clin Exp Pharmacol Physiol* 40: 765–773, 2013. doi:10.1111/1440-1681.12068.

46. **Oppenheim C, Mamou-Mani T, Sayegh N, de Blic J, Scheinmann P, Lallemand D.** Bronchopulmonary dysplasia: value of CT in identifying pulmonary sequelae. *AJR Am J Roentgenol* 163: 169–172, 1994. doi:10.2214/ajr.163.1.8010206.

47. **Price MM, Oskeritzian CA, Falanga YT, Harikumar KB, Allegood JC, Alvarez SE, Conrad D, Ryan JJ, Milstien S, Spiegel S.** A specific sphingosine kinase 1 inhibitor attenuates airway hyperresponsiveness and inflammation in a mast cell-dependent murine model of allergic asthma. *J Allergy Clin Immunol* 131: 501–511, 2013. doi:10.1016/j.jaci.2012.07.014.

48. **Rosenfeldt HM, Amrani Y, Watterson KR, Murthy KS, Panettieri RA Jr, Spiegel S.** Sphingosine-1-phosphate stimulates contraction of human airway smooth muscle cells. *FASEB J* 17: 1789–1799, 2003. doi:10.1096/fj.02-0836com.

49. **Royce SG, Nold MF, Bui C, Donovan C, Lam M, Lamanna E, Rudloff I, Bourke JE, Nold-Petry CA.** Airway remodeling and hyperreactivity in a model of bronchopulmonary dysplasia and their modulation by IL-1 receptor antagonist. *Am J Respir Cell Mol Biol* 55: 858–868, 2016. doi:10.1165/rcmb.2016-0031OC.

50. **Savani RC.** Modulators of inflammation in bronchopulmonary dysplasia. *Semin Perinatol* 42: 459–470, 2018. doi:10.1053/j.semperi.2018.09.009.

51. **Shah A, Xia L, Goldberg H, Lee KW, Quaggin SE, Fantus IG.** Thioredoxin-interacting protein mediates high glucose-induced reactive oxygen species generation by mitochondria and the NADPH oxidase, Nox4, in mesangial cells. *J Biol Chem* 288: 6835–6848, 2013. doi:10.1074/jbc.M112.419101.

52. **Siltanen M, Savilahti E, Pohjavuori M, Kajosaari M.** Respiratory symptoms and lung function in relation to atopy in children born preterm. *Pediatr Pulmonol* 37: 43–49, 2004. doi:10.1002/ppul.10402.

53. **Stoll BJ, Hansen NI, Bell EF, Shankaran S, Laptook AR, Walsh MC, Hale EC, Newman NS, Schibler K, Carlo WA, Kennedy KA, Poindexter BB, Finer NN, Ehrenkranz RA, Duara S, Sánchez PJ, O'Shea TM, Goldberg RN, Van Meurs KP, Faix RG, Phelps DL, Frantz ID III, Watterberg KL, Saha S, Das A, Higgins RD; Eunice Kennedy Shriver National Institute of Child Health and Human Development Neonatal Research Network.** Neonatal outcomes of extremely preterm infants from the NICHD Neonatal Research Network. *Pediatrics* 126: 443–456, 2010. doi:10.1542/peds.2009-2959.

54. **Stoll BJ, Hansen NI, Bell EF, Walsh MC, Carlo WA, Shankaran S, Laptook AR, Sánchez PJ, Van Meurs KP, Wyckoff M, Das A, Hale EC, Ball MB, Newman NS, Schibler K, Poindexter BB, Kennedy KA, Cotten CM, Watterberg KL, D'Angio CT, DeMauro SB, Truog WE, Devaskar U, Higgins RD; Eunice Kennedy Shriver National Institute of Child Health and Human Development Neonatal Research Network.** Trends in care practices, morbidity, and mortality of extremely preterm neonates, 1993–2012. *JAMA* 314: 1039–1051, 2015. doi:10.1001/jama.2015.10244.

55. **Tam A, Bates JH, Churg A, Wright JL, Man SF, Sin DD.** Sex-related differences in pulmonary function following 6 months of cigarette exposure: implications for sexual dimorphism in mild COPD. *PLoS One* 11: e0164835, 2016. doi:10.1371/journal.pone.0164835.

56. **Tibboel J, Joza S, Reiss I, de Jongste JC, Post M.** Amelioration of hyperoxia-induced lung injury using a sphingolipid-based intervention. *Eur Respir J* 42: 776–784, 2013. doi:10.1183/09031936.00092212.

57. **Tiddens HA, Hofhuis W, Casotti V, Hop WC, Hulsmann AR, de Jongste JC.** Airway dimensions in bronchopulmonary dysplasia: implications for airflow obstruction. *Pediatr Pulmonol* 43: 1206–1213, 2008. doi:10.1002/ppul.20928.

58. **Um-Bergström P, Hallberg J, Pourbazargan M, Berggren-Broström E, Ferrara G, Eriksson MJ, Nyrén S, Gao J, Lilja G, Lindén A, Wheelock AM, Melén E, Sköld CM.** Pulmonary outcomes in adults with a history of bronchopulmonary dysplasia differ from patients with asthma. *Respir Res* 20: 102, 2019. doi:10.1186/s12931-019-1075-1.

59. **Um-Bergström P, Hallberg J, Thunqvist P, Berggren-Broström E, Anderson M, Adenfelt G, Lilja G, Ferrara G, Sköld CM, Melén E.** Lung function development after preterm birth in relation to severity of bronchopulmonary dysplasia. *BMC Pulm Med* 17: 97, 2017. doi:10.1186/s12890-017-0441-3.

60. **van Mastrigt E, Logie K, Ciet P, Reiss IK, Duijts L, Pijnenburg MW, Tiddens HA.** Lung CT imaging in patients with bronchopulmonary dysplasia: a systematic review. *Pediatr Pulmonol* 51: 975–986, 2016. doi:10.1002/ppul.23446.

61. **Wang W, Hind T, Lam BWS, Herr DR.** Sphingosine 1-phosphate signaling induces SNAI2 expression to promote cell invasion in breast cancer cells. *FASEB J* 33: 7180–7191, 2019. doi:10.1096/fj.201801635R.

62. **Zeng Y, Yao X, Chen L, Yan Z, Liu J, Zhang Y, Feng T, Wu J, Liu X.** Sphingosine-1-phosphate induced epithelial-mesenchymal transition of hepatocellular carcinoma via an MMP-7/syndecan-1/TGF-β autocrine loop. *Oncotarget* 7: 63324–63337, 2016. doi:10.18632/oncotarget.11450.

63. **Zhao Y, Kalari SK, Usatyuk PV, Gorshkova I, He D, Watkins T, Brindley DN, Sun C, Bittman R, Garcia JG, Berdyshev EV, Natarajan V.** Intracellular generation of sphingosine 1-phosphate in human lung endothelial cells: role of lipid phosphate phosphatase-1 and sphingosine kinase 1. *J Biol Chem* 282: 14165–14177, 2007. doi:10.1074/jbc.M701279200.

64. **Zysman-Colman Z, Tremblay GM, Bandeali S, Landry JS.** Bronchopulmonary dysplasia - trends over three decades. *Paediatr Child Health* 18: 86–90, 2013. doi:10.1093/pch/18.2.86.